Taylor & Francis
Taylor & Francis Group

Geophysical & Astrophysical Fluid Dynamics

ISSN: 0309-1929 (Print) 1029-0419 (Online) Journal homepage: http://www.tandfonline.com/loi/ggaf20

Convection of a fluid with strongly temperature and pressure dependent viscosity

A. C. Fowler, P. D. Howell & Tania S. Khaleque

To cite this article: A. C. Fowler, P. D. Howell & Tania S. Khaleque (2016) Convection of a fluid with strongly temperature and pressure dependent viscosity, Geophysical & Astrophysical Fluid Dynamics, 110:2, 130-165

To link to this article: http://dx.doi.org/10.1080/03091929.2016.1146264

Published online: 10 Mar 2016.

Submit your article to this journal

View related articles

View Crossmark data

Full Terms & Conditions of access and use can be found at
http://www.tandfonline.com/action/journalInformation?journalCode=ggaf20

Download by: [89.234.79.13] **Date:** 10 March 2016, At: 03:45

GEOPHYSICAL AND ASTROPHYSICAL FLUID DYNAMICS, 2016
VOL. 110, NO. 2, 130–165
http://dx.doi.org/10.1080/03091929.2016.1146264

Taylor & Francis
Taylor & Francis Group

Convection of a fluid with strongly temperature and pressure dependent viscosity

A. C. Fowler[a,b], P. D. Howell[b] and Tania S. Khaleque[b]

[a]MACSI, University of Limerick, Limerick, Ireland; [b]OCIAM, University of Oxford, Oxford, UK

ABSTRACT

Plate tectonics on the Earth is a surface manifestation of convection within the Earth's mantle, a subject which is as yet improperly understood, and it has motivated the study of various forms of buoyancy-driven thermal convection. The early success of the high Rayleigh number constant viscosity theory was later tempered by the absence of plate motion when the viscosity is more realistically strongly temperature dependent, and the process of subduction represents a continuing principal conundrum in the application of convection theory to the Earth. A similar problem appears to arise if the equally strong pressure dependence of viscosity is considered, since the classical isothermal core convection theory would then imply a strongly variable viscosity in the convective core, which is inconsistent with results from post-glacial rebound studies. In this paper we address the problem of determining the asymptotic structure of high Rayleigh number convection when the viscosity is strongly temperature and pressure dependent, i.e. *thermobaroviscous*. By a method akin to lid-stripping, we are able to extend numerical computations to extremely high viscosity contrasts, and we show that the convective cells take the form of narrow, vertically-oriented fingers. We are then able to determine the asymptotic structure of the solution, and it agrees well with the numerical results. Beneath a stagnant lid, there is a vigorous convection in the upper part of the cell, and a more sluggish, higher viscosity flow in the lower part of the cell. We then offer some comments on the possible meaning and interpretation of these results for planetary mantle convection.

ARTICLE HISTORY
Received 28 April 2015
Accepted 21 January 2016

KEYWORDS
Mantle convection; fast thermobaroviscous convection; variable viscosity

Downloaded by [89.234.79.13] at 03:45 10 March 2016

1. Introduction

Since the final acceptance of the theory of plate tectonics in the 1960s, the study of high Rayleigh number convection has enjoyed a long history. The plate tectonic motions are a surface manifestation of underlying convective currents in the (solid) Earth's mantle, driven by a combination of radioactive heat release and planetary cooling, and the simplest model to study these motions is that of a Rayleigh–Bénard convection cell of a viscous fluid at high Rayleigh number. Assessments of the mantle viscosity beneath the relatively rigid lithosphere indicate a relatively uniform viscosity[1] of about 10^{21} Pa s (Haskell 1935, Cathles

CONTACT A. C. Fowler fowler@maths.ox.ac.uk

[1]By this we mean that the variation of viscosity in the mantle may be some two or three orders of magnitude, but not 10 or 15.

© 2016 Taylor & Francis

Downloaded by [89.234.79.13] at 03:45 10 March 2016

1975), and subsequent studies have not essentially altered that conclusion (e.g. Paulson *et al.* 2007). In consequence, early studies of mantle convection assumed a constant viscosity, and both numerical and analytic studies appeared to give a satisfactory explanation for plate tectonic observations on the Earth (Turcotte and Oxburgh 1967, Moore and Weiss 1973, Roberts 1979, Jarvis and Peltier 1982, Jimenez and Zufiria 1987).

However, it became clear that these results were not so simply applicable as might be wished, for a number of reasons. While the active plate tectonic style of convection on Earth resembles these earlier studies, such convection is not seen on the nearest analogues, Venus and Mars, although there is evidence of active tectonics on Venus some 500 Ma ago (Schaber *et al.* 1992). It turns out that convection on Venus and Mars is more what one would expect, and the Earth's active style is anomalous.

The reason for this has to do with the rheology of mantle rocks. It is well known that the effective viscosity of the Earth is a strong function of temperature, pressure and stress. The temperature and stress dependence are well documented experimentally; the pressure dependence is less constrained, but reasonable estimates for all these dependences are available (Kirby 1983, Karato and Wu 1993, Yamazaki and Karato 2001). It is a consequence of the temperature dependence of the viscosity that the cold upper thermal boundary layer, which is in fact the lithosphere, is extremely viscous, and this causes it to be effectively rigid and immobile. The resulting form of convection is called stagnant lid convection, and presumably corresponds to what is seen on Mars and present day Venus. The active style of tectonics on Earth is generally thought to be a consequence of weakening at high stresses, due either to stress-dependent viscosity or to plastic yielding (Bercovici 1993, 2003, Fowler 1993b, Tackley 1998, 2000a,b, Fowler and O'Brien 2003).

The boundary layer theory of high Rayleigh number constant viscosity convection was developed by several authors, notably Turcotte and Oxburgh (1967), Roberts (1979) and Vynnycky and Masuda (2013), and extended more or less successfully to temperature-dependent viscosity by Morris and Canright (1984) and Fowler (1985a). A feature of both sets of analyses is that the rapid convection in the interior of the cell causes the temperature to be isothermal (and thus, for the temperature-dependent viscosity case, isoviscous). In seeking to extend the asymptotic theory to the more realistic temperature and pressure dependent viscosity case (what we term the thermobaroviscous case), the theory encounters a significant problem, however. While rapid convection promotes an isothermal interior, this generally leads, in a thermobaroviscous fluid, to an interior viscosity which increases dramatically with depth, a result which is at odds with the observed, relatively constant, sub-lithospheric viscosity in the mantle. It was pointed out by Sammis *et al.* (1977) that a more realistic consideration of mineral properties, together with an adiabatic temperature gradient, could lead to a relatively constant mantle viscosity, but it was then pointed out by Fowler (1983) that this led to anomalously low adiabatic temperatures near the core-mantle boundary (CMB), and the consequent necessity for a very large temperature jump in the resultant basal thermal boundary layer, something which is not apparently consistent with the dynamics of strongly variable viscosity convection. It was suggested by Fowler (1993a) that a resolution of this issue might consist of rapid thermobaroviscous convection taking the form of a rapidly convecting interior which was isoviscous rather than isothermal. However, sporadic efforts to elucidate such a structure have since then failed.

When analytic methods fail, one looks to numerical computation to lead the way. The history of computational studies of variable viscosity convection is an interesting one.

Downloaded by [89.234.79.13] at 03:45 10 March 2016

Confronted with the goal of computing convective solutions in which the potential viscosity variations are by factors in the region of 10^{50}, the challenge is to approach such extreme contrasts sufficiently that the correct asymptotic structure is reached. Very early attempts foundered on the computational difficulty which extreme viscosity contrasts caused. In the 1980s, Christensen and his co-workers (Christensen 1984a,b, 1985, Christensen and Yuen 1984, 1985, Christensen and Harder 1991) were able to compute models with viscosity contrasts up to about 10^6. Solomatov and his co-workers were later able to extend these results up to viscosity contrasts around 10^{15} (Moresi and Solomatov, 1995, 1998, Solomatov 1996, Reese *et al.* 1999, Reese and Solomatov 2002). One would naturally expect that such extreme values attain the structure of the asymptotic limit, and while this seems to be true for temperature-dependent viscosity, it is not obviously true, as we shall see, for temperature- and pressure-dependent viscosity. The state of the art in computational models now is that there is no effort to compute results for more extreme viscosity contrasts, rather the research effort is devoted to the inclusion of more realistic physical constraints, for example phase changes, spherical geometry, etc., or to applications of previously developed models; see for example Orth and Solomatov (2011), Stein and Hansen (2013), Deschamps *et al.* (2015).

The situation we have is this. The viscosity of silicate rocks is usually taken as proportional to $\exp\left(H^*/RT\right)$, where the activation enthalpy $H^* = E^* + pV^*$, E^* is the activation energy, p is pressure, and V^* is activation volume. The pressure at the CMB is 140 GPa, so that if $V^* = [V]\,\mathrm{cm}^3\,\mathrm{mol}^{-1}$, then $pV^* = 140[V]\,\mathrm{kJ\,mol}^{-1}$. Similarly, we write $E^* = [E]\,\mathrm{kJ\,mol}^{-1}$. By contrast, for an assumed CMB temperature of 4000 K, $RT = 33.2\,\mathrm{kJ\,mol}^{-1}$. Typical values of $[E]$ are in the range 200–500, while estimates of $[V]$ range from 2 to 15, and thus $p[V] \gtrsim 280$. It is because $E^* \sim pV^* \gg RT$ that we know that pressure dependence of viscosity in the Earth's mantle is as significant as temperature dependence. It is this dependence which prompts our study. Despite this, near-adiabatic temperatures, as one might expect from high Rayleigh number convection, may lead to viscosity profiles which are consistent with observation (Sammis *et al.* 1977). Further discussion of the implications of this is given in section 4.

2. The Boussinesq model of convection

We consider two-dimensional convection in a box of depth d, as shown in figure 1; the width of the box will be specified in due course. The Boussinesq model of convection assumes that density variation is only important in the buoyancy term of the momentum equation, so that mass conservation takes the form of the incompressibility condition, and equally we take the dissipation number

$$D = \frac{\alpha g d}{c_p} \tag{1}$$

to be zero, where α is the thermal expansion coefficient, g is the acceleration due to gravity, and c_p is the specific heat. Actually, $D = O(1)$ in the mantle, and the assumption that $D = 0$ corresponds to neglecting the adiabatic term in the energy equation. A discussion of the important effect of a non-zero dissipation number is given in the discussion, section 4. Neglect of D also means that viscous dissipation is neglected, which is mostly a good approximation. Suitable equations to describe the motion are then

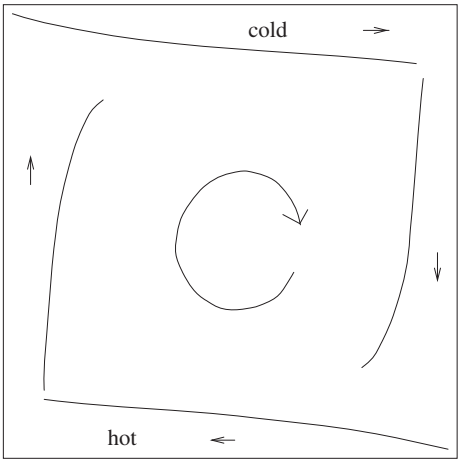

Figure 1. Schematic representation of boundary layer convection.

Downloaded by [89.234.79.13] at 03:45 10 March 2016

$$
\begin{aligned}
u_x + w_z &= 0\,, & \rho &= \rho_m\big[1-\alpha(T-T_{\text{ast}})\big]\,,\\
p_x &= \tau_{1x} + \tau_{3z}\,, & p_z &= \tau_{3x} - \tau_{1z} - \rho g\,,\\
\tau_1 &= \eta u_x\,, & \tau_3 &= \eta(u_z + w_x)\,,\\
& & T_t + uT_x + wT_z &= \kappa\nabla^2 T\,,\\
\tau^2 &= \tau_1^2 + \tau_3^2\,, & \eta &= \frac{1}{2A\tau^{n-1}}\exp\left[\frac{E^* + pV^*}{RT}\right],
\end{aligned}
\tag{2}
$$

where letter subscripts denote partial derivatives. Here, (u, w) are the components of velocity, p is pressure, τ_1 and τ_3 are longitudinal and shear components of the deviatoric stress, ρ is density, T is temperature, $2\tau^2$ is the second stress invariant, and η is the viscosity, assumed here to be a general power law of strain softening type. Other constants in the model are an asthenospheric temperature T_{ast}, which will be specified in due course, the thermal diffusivity κ, the rheological rate factor A, the perfect gas constant R, the activation energy E^*, the activation volume V^*, and the flow law exponent n.

The present model ignores internal heating, so that convection is driven by heating from below, and we prescribe boundary conditions to be those for free slip and prescribed temperature:

$$
\begin{aligned}
u = \tau_3 = 0, &\qquad T_x = 0 \quad \text{on} \quad x = 0,\, l,\\
w = \tau_3 = 0, &\qquad T = T_b \quad \text{on} \quad z = 0,\\
w = \tau_3 = 0, &\qquad T = T_s \quad \text{on} \quad z = d;
\end{aligned}
\tag{3}
$$

the depth of the convection cell is d and its width is l.

We define a stream function ψ by

$$
u = -\psi_z, \qquad w = \psi_x, \tag{4}
$$

and then we make the equations dimensionless by scaling the variables as

$$\psi \sim \kappa, \qquad T \sim T_b, \qquad \eta \sim \eta_m, \qquad \tau, \tau_1, \tau_3 \sim \frac{\eta_m \kappa}{d^2},$$
$$t \sim \frac{d^2}{\kappa}, \qquad x, z \sim d, \qquad p - \rho_m g(d - z) \sim \frac{\eta_m \kappa}{d^2}, \tag{5}$$

where η_m has yet to be specified.

This leads to the dimensionless set

$$p_x = \tau_{1x} + \tau_{3z}, \qquad p_z = \tau_{3x} - \tau_{1z} + Ra\,(T - T_a),$$
$$\tau_1 = -2\eta\psi_{xz}, \qquad \tau_3 = \eta(\psi_{xx} - \psi_{zz}),$$
$$T_t + \psi_x T_z - \psi_z T_x = \nabla^2 T,$$
$$\tau^2 = \tau_1^2 + \tau_3^2, \qquad \eta = \frac{\Lambda}{\tau^{n-1}} \exp\left[\frac{1 - T + \mu(1 - z - T)}{\varepsilon T}\right]. \tag{6}$$

Note that for a clockwise convection cell as shown in figure 1, $\psi > 0$.

The parameters in (6) are then defined by

$$Ra = \frac{\alpha T_b \rho_m g d^3}{\eta_m \kappa}, \qquad \varepsilon = \frac{RT_b}{E^*}, \qquad \mu = \frac{\rho_m g d V^*}{E^*},$$
$$T_a = \frac{T_{\text{ast}}}{T_b}, \qquad \Lambda = \frac{1}{2A\eta_m^n}\left(\frac{d^2}{\kappa}\right)^{n-1} \exp\left[\frac{E^* + \rho_m g d V^*}{RT_b}\right]. \tag{7}$$

Assumed values for the parameters of the problem are given in table 1, and typical values of the dimensionless parameters are given in table 2. In this paper, we consider only Newtonian rheologies, for which $n = 1$, and then we can choose $\Lambda = 1$, thus defining

$$\eta_m = \frac{1}{2A} \exp\left[\frac{E^* + \rho_m g d V^*}{RT_b}\right] \tag{8}$$

as the mantle viscosity at the CMB. The more laborious procedure of choosing Λ when $n \neq 1$ is discussed by Fowler and O'Brien (2003, Appendix A). The value of T_a is chosen later, as its determination forms part of the solution.

Before beginning our study, it is worth emphasising its shortcomings, at least as regards its applicability to the Earth or other terrestrial planets. We have chosen to study steady, two-dimensional convection in a Cartesian frame; we have ignored internal heating, have assumed zero isothermal compressibility, ignored the adiabatic temperature rise term, and we have assumed a stress-independent rheology described by constant activation energy and volume of a material which undergoes no phase changes. Various quantities, in particular α and V^*, are assumed constant, and the ramifications of this are discussed in section 4. Of course, none of these assumptions is valid, but we have made them in order to obtain a problem whose analysis is tractable.

We comment on two of these assumptions which may be thought to be the most relevant. Firstly, internal heating is thought to be significant in the Earth's mantle, and it might be thought that if this is the case, the dynamics of the motion would be quite different. It turns

Downloaded by [89.234.79.13] at 03:45 10 March 2016

Table 1. Parameter values relevant to the Earth. Estimates for the activation volume vary between about 5 and 20 $cm^3\ mol^{-1}$; our particular choice here is to give a mantle viscosity η_m similar to that which is observed. The values of E^* and V^* are appropriate for the upper mantle, but lower mantle values may be lower, as discussed in section 4. Present estimates for T_b are closer to 4000 K, but in any case the values here are meant to be suggestive rather than absolute.

Symbol	Meaning	Typical value
A	Viscous rate constant	$10^5\ MPa^{-n}\ s^{-1}$
d	Mantle depth	3000 km
E^*	Activation energy	$525\ kJ\ mol^{-1}$
g	Gravitational acceleration	$10\ m\ s^{-2}$
n	Flow law exponent	3.5
R	Universal gas constant	$8.3\ J\ mol^{-1}\ K^{-1}$
T_b	Basal temperature	3500 K
T_s	Surface temperature	300 K
V^*	Activation volume	$7\ cm^3\ mol^{-1}$
α	Thermal expansion coefficient	$3 \times 10^{-5}\ K^{-1}$
η_m	Mantle viscosity	1.3×10^{21} Pa s
κ	Thermal diffusivity	$10^{-6}\ m^2\ s^{-1}$
ρ_m	Typical mantle density	$4 \times 10^3\ kg\ m^{-3}$

Table 2. Dimensionless parameter values, using the constants in table 1. The values of T_a and η_a are computed using (23). Note that the corresponding value of T_{ast} is 1540 K.

Symbol	Meaning	Typical value
Ra	Rayleigh number	3.2×10^7
T_0	Dimensionless surface temperature	0.09
T_a	Dimensionless asthenosphere temperature	0.44
ε	Viscous temperature number	0.055
η_a	Dimensionless asthenosphere viscosity	2.8×10^{-3}
μ	Viscous pressure number	1.6

out, perhaps surprisingly, that this appears at first sight not to be the case. The reasons for this are discussed thoroughly in section 4.

In our analysis, we will make much of the fact that the viscosity given by $(2)_9$ is a strong function of temperature and pressure. The activation enthalpy $H^* = E^* + pV^*$ (equivalently, for an isentropic, i.e. adiabatic, flow we may use the Gibbs free energy $G^* = E^* + pV^* - TS$) varies with pressure in the mantle, but the variation is not linear, because the activation volume V^* decreases with increasing depth. Various studies have suggested that this decrease, combined with an increasing adiabatic temperature, leads to a variation of viscosity in the mantle which is not as dramatic as our analysis would suggest. We offer further discussion of this point in section 4.

3. Temperature and pressure dependent viscosity

In order to obtain simulations relevant to the Earth, extremely high viscosity contrasts are necessary. The surface to base contrast of viscosity for the parameter values in table 2 is of the order of 10^{67}, for example. Computations have been done previously for variable viscosity contrasts up to 10^{15}, but surprisingly, this is not sufficient to establish a clear asymptotic limit for the flow.

Downloaded by [89.234.79.13] at 03:45 10 March 2016

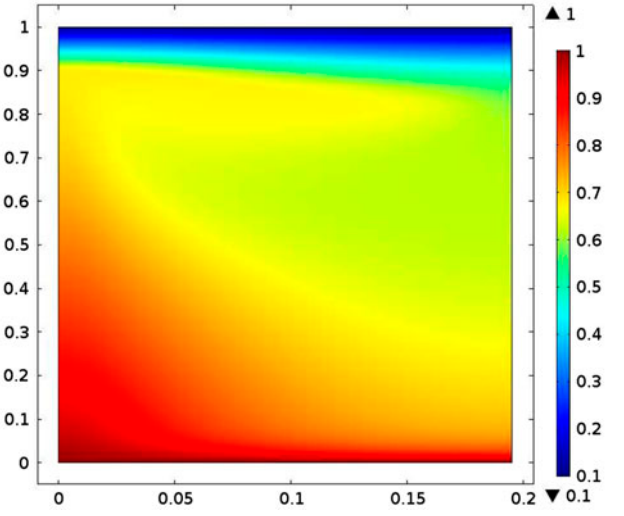

Figure 2. Colour plot (red warm, blue cold) of temperature for a box of width 3ε at values $Ra = 10^7$, $\mu = 1$ and $\varepsilon = 0.065$ and with $T_0 = 0.1$. The top to bottom viscosity contrast for these values is 2.8×10^{53}.

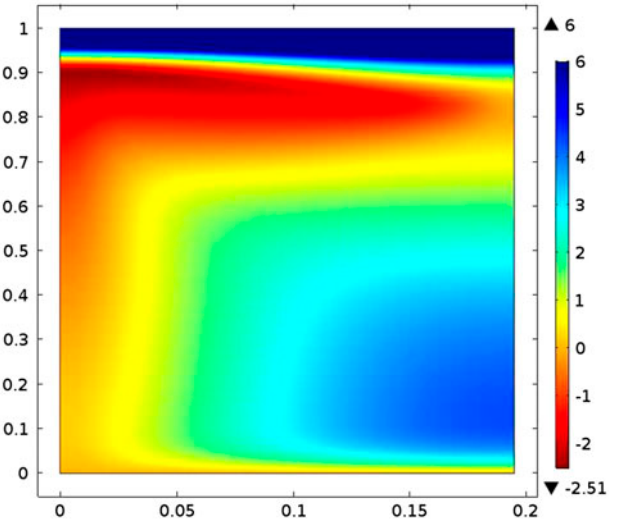

Figure 3. Colour plot of dimensionless viscosity (red low, blue high) for the box of figure 2 at the same parameter values. The calculations were done with viscosity as defined in (9), with a cut-off at $\eta = 10^6$. The colour scale gives $\log_{10} \eta$.

In our more recent attempt to solve the problem, we have been guided by a series of numerical experiments (Khaleque *et al.* 2015). These have overcome the difficulties associated with high viscosity contrasts by means of a trick based on the fact that, like strongly temperature-dependent viscous convection, most of the viscosity variation occurs in a stagnant lid, in which the velocity is essentially zero. We can then simulate the sub-lid convection field accurately by cutting off the dimensionless viscosity at a sufficiently high value that the lid thickness, which essentially only depends on the interaction of the

Downloaded by [89.234.79.13] at 03:45 10 March 2016

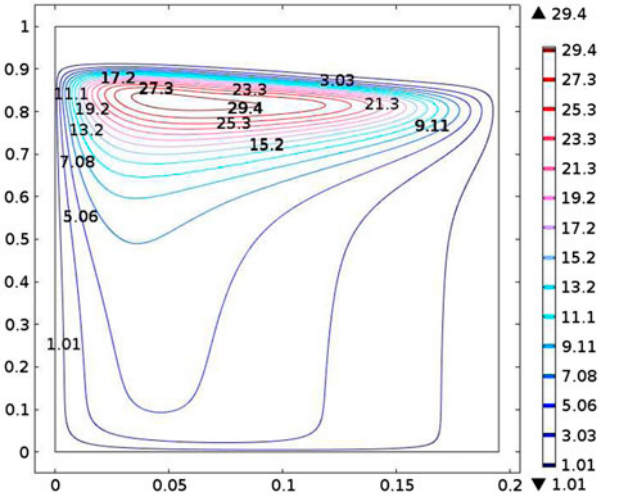

Figure 4. Contours of stream function ψ for the calculations in figure 2.

Downloaded by [89.234.79.13] at 03:45 10 March 2016

lid temperature with the underlying convecting flow, is unaffected. In practice a cut-off at a dimensionless viscosity of 10^6 was sufficient. The resulting calculations do not yield accurate values for the stresses in the lid, but they do yield accurate solutions elsewhere. Further details are described in the thesis of Khaleque (2015).

The essential clue to the problem of strong thermobaroviscous convection is the discovery, in the course of these numerical experiments, that convection in a square cell becomes untenable at a viscosity contrast of $\sim 10^{30}$. Around this value, the convective flow breaks into three cells, and this revelation led to the idea that the way the flow structure copes with the increasing pressure dependence of the viscosity is by restricting the cells to have narrow width. Following this idea, we were able to solve for convective flow in increasingly narrow cells as the viscosity contrast was increased. Figures 2–4 show an example of a computation performed using COMSOL Multiphysics (Khaleque *et al.* 2015) with a viscosity contrast of order 10^{53} in a box with an approximate aspect ratio of 1:5; the horizontal coordinate is stretched to illuminate the flow structure. These figures are discussed further below. However, while there is clearly a stagnant lid in the cell, it is clear that the convecting part of the flow is neither isothermal nor isoviscous. Note also the relative increase in viscosity from the "upper mantle" to the "lower mantle" by a factor ranging from 10^2 at the left to 10^6 at the right. Such a result is consistent with observationally derived inferences of upper mantle/lower mantle viscosity contrast (e.g. Mitrovica and Forte 2004).

3.1. *Rescaling for narrow cells*

As we choose to ignore the stress dependence of the viscosity, we take $\Lambda = n = 1$ in (6), so that the model set of equations which we study (and whose solutions are shown in figures 2–4) is

$$p_x = \tau_{1x} + \tau_{3z}, \qquad p_z = \tau_{3x} - \tau_{1z} - Ra\,(T_a - T),$$
$$\tau_1 = -2\eta\psi_{xz}, \qquad \tau_3 = \eta(\psi_{xx} - \psi_{zz}),$$

$$T_t + \psi_x T_z - \psi_z T_x = \nabla^2 T,$$
$$\eta = \exp\left[\frac{1 - T + \mu(1 - z - T)}{\varepsilon T}\right]. \tag{9}$$

Our presumption is that the preferred scale width for the convection cells is $\sim \varepsilon$, and this suggests two forms of rescaling.[2] We call the first of these the *upper core scaling*, and it is given by

$$x = \varepsilon X, \qquad z = 1 - \varepsilon Z, \qquad t \sim \varepsilon^2. \tag{10}$$

In terms of these, the upper core equations are

$$p_X = \tau_{1X} - \tau_{3Z}, \qquad -p_Z = \tau_{3X} + \tau_{1Z} - \varepsilon Ra\,(T_a - T),$$
$$\tau_1 = \frac{2\eta}{\varepsilon^2}\psi_{XZ}, \qquad \tau_3 = \frac{\eta}{\varepsilon^2}(\psi_{XX} - \psi_{ZZ}),$$
$$T_t + \psi_Z T_X - \psi_X T_Z = \nabla^2 T,$$
$$\eta = \exp\left[\frac{1 - T + \mu(\varepsilon Z - T)}{\varepsilon T}\right]. \tag{11}$$

Note that the other dimensionless variables have yet to be scaled appropriately.

The *lower core* scaling is similar, but retains the original z scaling; we will come to it in due course.

The boundary conditions that are to be applied are

$$\psi = \tau_3 = 0, \qquad T_X = 0 \quad \text{on} \quad X = 0, a,$$
$$\psi = \tau_3 = 0, \qquad T = 1 \quad \text{on} \quad z = 0,$$
$$\psi = \tau_3 = 0, \qquad T = T_0 \quad \text{on} \quad z = 1, \tag{12}$$

where $a = l/\varepsilon d$ is the scaled width of the convection cell.

The essence of our discussion follows from the assertion that the flow consists of two parts, an "upper mantle" flow in which $1 - z \sim \varepsilon$, and a "lower mantle" part in which $z \sim O(1)$. The upper mantle behaviour is somewhat similar to that of purely temperature-dependent viscous convection.

3.2. Heat flux

Before beginning, we derive a useful condition on the surface heat flux. In the absence of convection, the conductive temperature is just

$$T = 1 - (1 - T_0)z, \tag{13}$$

[2] More generally, we may take a small aspect ratio ν, and then we find that the choice $\nu = \varepsilon$ is a distinguished limit for $\mu = O(1)$ which allows exponential decline of the viscosity in the upper part of the convective cell. More generally, we might have $\nu = \varepsilon/\mu$, but the simpler choice is sufficient.

Downloaded by [89.234.79.13] at 03:45 10 March 2016

and we therefore define the Nusselt number Nu to be the average surface heat flux relative to this, thus

$$Nu = \frac{1}{(1-T_0)a}\int_0^a \left(-\left.\frac{\partial T}{\partial z}\right|_{z=1}\right) \mathrm{d}X = \frac{1}{\varepsilon(1-T_0)a}\int_0^a \left.\frac{\partial T}{\partial Z}\right|_{Z=0} \mathrm{d}X. \tag{14}$$

In a steady state (with which we will be mostly concerned), exact integration of $(11)_5$ then shows that

$$\int_{X=0}^{X=a} T\mathrm{d}\psi - T_X \mathrm{d}Z + T_Z \mathrm{d}X = \varepsilon a(1-T_0)Nu, \tag{15}$$

where the integral is along any curve from $X = 0$ to $X = a$.

3.3. Stagnant lid

Our analysis in the upper mantle follows the reasoning of Fowler (1985a) in making an effort to determine the appropriate scales.

There is a stagnant lid, which we may identify with the *lithosphere*, in which $\psi \ll 1$, and heat transfer is purely conductive. We denote the lid base by

$$Z = \gamma s(X), \tag{16}$$

and we presume that $\varepsilon\gamma \ll 1$, so that the lid is thin, relative to the cell depth. A self-consistent determination of γ is one of the harder parts of this theory, but numerical solutions suggest that $\gamma \sim 1$, and so we will formally assume

$$\gamma = 1. \tag{17}$$

Later we make some comments on other possibilities. In this case, the aspect ratio of the lid is O(1), and therefore the temperature in the lid is determined by solving the heat conduction equation, since thermal advection is negligible. Specifically, we write

$$T = T_0 + (T_a - T_0)\Theta, \tag{18}$$

where T_a is the asthenospheric temperature at the base of the lid, which we take to be constant, as we suppose the base of the lid is essentially determined by an isoviscosity contour. The problem to solve for Θ is then

$$\begin{aligned} &\nabla^2\Theta = 0, \\ \Theta = 0 \qquad &\text{on} \quad Z = 0, \\ \Theta = 1, \qquad \Theta_Z = G(X) \qquad &\text{on} \quad Z = s, \\ \Theta_X = 0 \qquad &\text{on} \quad X = 0, a. \end{aligned} \tag{19}$$

Note that integration over the lid implies from (15) that

$$Nu = \frac{(T_a - T_0)}{\varepsilon a(1-T_0)}\int_0^a (1+s'^2)\, G(X)\, \mathrm{d}X. \tag{20}$$

Downloaded by [89.234.79.13] at 03:45 10 March 2016

3.4. Asthenosphere

Below the stagnant lid there is a shear layer, in which the temperature switches from its conductive profile to an adiabatic profile. We term this layer the asthenosphere, which is its dynamical counterpart in plate tectonic models of mantle convection. It is referred to by Fowler (1985a) as a delamination layer. In this layer we introduce the scales

$$T = T_a + \varepsilon\theta, \qquad Z = s(X) + \varepsilon\zeta, \qquad \psi \sim \frac{1}{\varepsilon}, \qquad \eta \sim \eta_a = \varepsilon^8 Ra, \tag{21}$$

where also

$$\eta_a = \exp\left[\frac{1-(1+\mu)T_a}{\varepsilon T_a}\right], \tag{22}$$

so that

$$T_a = \frac{1}{1+\mu+\varepsilon\ln(\varepsilon^8 Ra)}, \tag{23}$$

which provides the definition of T_a. The choice of scales is made by balancing the terms in (11) in a similar manner to Fowler (1985a). For the values we mostly use in our computations, $\varepsilon = 0.065$, $\mu = 1$, $Ra = 10^7$, we have $T_a \approx 0.615$.

From (22) we find

$$\eta = \exp\left[\frac{\mu T_a Z - \theta}{T_a(T_a+\varepsilon\theta)}\right] \approx \exp\left[\frac{-\theta + \mu T_a s}{T_a^2}\right], \tag{24}$$

and the appropriate scales for the stresses in the shear layer are then

$$p,\ \tau_1,\ \tau_3 \sim \varepsilon^3 Ra. \tag{25}$$

Using these scales, the governing equations in the asthenosphere are (assuming steady state)

$$\begin{aligned}
\varepsilon p_X - s' p_\zeta &= \varepsilon\tau_{1\zeta} - s'\tau_{1\zeta} - \tau_{3\zeta},\\
-p_\zeta &= \varepsilon\tau_{3X} - s'\tau_{3\zeta} + \tau_{1\zeta} + \theta,\\
\tau_1 &= 2\eta\left[\varepsilon\psi_{X\zeta} - s'\psi_{\zeta\zeta}\right],\\
\tau_3 &= \eta\left[\varepsilon^2\psi_{XX} - \varepsilon\left(2s'\psi_{X\zeta} + s''\psi_\zeta\right) - (1-s'^2)\psi_{\zeta\zeta}\right],\\
\psi_\zeta\theta_X - \psi_X\theta_\zeta &= (1+s'^2)\theta_{\zeta\zeta} - \varepsilon\left(2s'\theta_{X\zeta} + s''\theta_\zeta\right) + \varepsilon^2\theta_{XX},\\
\eta &\approx \exp\left[\frac{\mu s}{T_a} - \frac{\theta}{T_a^2}\right],
\end{aligned} \tag{26}$$

with boundary conditions

$$\begin{aligned}
\psi \to 0, \quad \theta_\zeta \sim (T_a - T_0)G \qquad &\text{as} \quad \zeta \to -\infty,\\
\tau_3,\ \theta \to 0 \qquad &\text{as} \quad \zeta \to \infty.
\end{aligned} \tag{27}$$

Downloaded by [89.234.79.13] at 03:45 10 March 2016

Downloaded by [89.234.79.13] at 03:45 10 March 2016

We put $\varepsilon = 0$; the equations (26) reduce to

$$\begin{aligned} -s'p_\zeta &= -s'\tau_{1\zeta} - \tau_{3\zeta}, \qquad -p_\zeta = -s'\tau_{3\zeta} + \tau_{1\zeta} + \theta, \\ \tau_1 &= -2\eta s'\psi_{\zeta\zeta}, \qquad \tau_3 = -\eta(1-s'^2)\psi_{\zeta\zeta}, \\ \psi_\zeta\theta_X - \psi_X\theta_\zeta &= (1+s'^2)\theta_{\zeta\zeta}, \\ \eta &\approx \exp\left[\frac{\mu s}{T_a} - \frac{\theta}{T_a^2}\right], \end{aligned} \tag{28}$$

which are analogous to those studied by Fowler (1985a), and for which a similarity solution exists, given by

$$\begin{aligned} \theta &= T_a^2 g(\xi), \qquad \psi = \frac{T_a^8}{(T_a-T_0)^3}\frac{s'}{G^3(1+s'^2)^2}\exp\left[-\frac{\mu s}{T_a}\right]f(\xi), \\ \xi &= \frac{(T_a-T_0)G(X)\zeta}{T_a^2}, \qquad \tau_3 = \frac{T_a^4 s'(1-s'^2)}{(T_a-T_0)G(1+s'^2)^2}h(\xi), \end{aligned} \tag{29}$$

where

$$h' + g = 0, \qquad f'' = -h\,\mathrm{e}^g, \qquad g'' + Afg' = 0, \tag{30}$$

the boundary conditions are

$$g(\infty) = h(\infty) = 0, \qquad f(-\infty) = 0, \qquad g'(-\infty) = 1, \tag{31}$$

and s satisfies

$$\frac{1}{G(1+s'^2)}\left[\frac{s'}{G^3(1+s'^2)^2}\exp\left(-\frac{\mu s}{T_a}\right)\right]' = \beta, \tag{32}$$

where

$$\beta = \frac{A(T_a-T_0)^4}{T_a^{10}}. \tag{33}$$

As explained by Fowler (1985a), the value of A is determined by the solution of (30), and is given by $A = 0.087$ (Fowler 2011, p. 509). With $T_a = 0.615$ and $T_0 = 0.1$ for example, $\beta = 0.79$.

3.5. Lid temperature computation

We now return to the intricate problem of computing the lid temperature. The coupled system (19) and (32) must generally be solved numerically. It is a complicated free boundary problem. If s is known, then it is straightforward to calculate G from (19), and then (32) provides a second order differential equation for s. This provides the nucleus of an iterative procedure for the solution. The issue of boundary conditions for s is discussed later.

We solve the coupled system (19) and (32) numerically as follows. We define the conjugate function

$$\chi = \frac{1}{C}\int_{(0,0)}^{(X,Z)} \left[\Theta_Z\,\mathrm{d}X - \Theta_X\,\mathrm{d}Z\right], \tag{34}$$

well-defined since Θ satisfies Laplace's equation; C is defined by the requirement that $\Theta = 1$ on $Z = s$, which implies

$$C = 1 \Big/ \int_0^s \chi_X \, \mathrm{d}Z. \tag{35}$$

We define the arc length σ on $Z = s$, so that

$$\frac{\mathrm{d}X}{\mathrm{d}\sigma} = \cos\phi, \qquad \frac{\mathrm{d}s}{\mathrm{d}\sigma} = \sin\phi, \qquad s_X = \tan\phi; \tag{36}$$

the normal to $Z = s$ is $(-\sin\phi, \cos\phi)$, and it follows that χ satisfies

$$\begin{aligned} \nabla^2\chi &= 0, \\ \chi &= 0 \quad \text{on} \quad X = 0, \\ \chi &= 1 \quad \text{on} \quad X = a, \\ \chi_Z &= 0 \quad \text{on} \quad Z = 0, \\ \chi_Z - s_X\,\chi_X &= 0 \quad \text{on} \quad Z = s. \end{aligned} \tag{37}$$

(The constant value of χ at $X = a$ is arbitrary, as can be seen from (34) and (35).)

The free boundary equation (32) to determine s can be written as

$$\frac{\mathrm{d}}{\mathrm{d}\sigma}\left[\frac{s_X}{G^3(1+s_X^2)^2}\exp\left(-\frac{\mu s}{T_a}\right)\right] = \beta G \sec\phi\,; \tag{38}$$

using the boundary condition $(37)_5$, we also have

$$\frac{\mathrm{d}\chi}{\mathrm{d}\sigma} = \frac{G}{C}\sec\phi \tag{39}$$

on $Z = s$, and thus, using also that

$$G = C\chi_X\big|_s, \tag{40}$$

integration of (38) yields

$$\frac{s_X}{(1+s_X^2)^2}\exp\left(-\frac{\mu s}{T_a}\right) = \beta D, \tag{41}$$

where

$$D = C^4\chi\,\chi_X^3, \tag{42}$$

and χ and χ_X are evaluated on $Z = s$.

The advantage of this formulation is that it cleanly separates the determination of χ and s, providing a simple way (in principle!) of iterating towards a solution. To be specific, we would solve (37) for given s to determine χ; then we solve (41) for s, providing an update, and then we would iterate the process, on the assumption that the iteration converges. In practice, the solution is so sensitive that we adopt an alternative strategy.

Downloaded by [89.234.79.13] at 03:45 10 March 2016

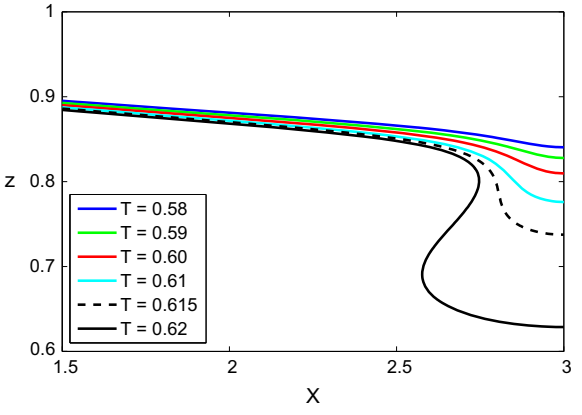

Figure 5. Plume formation at the end of the asthenosphere. As indicated, the contours are those of constant temperature $T = 0.58$, $T = 0.59$, $T = 0.60$, $T = 0.61$, $T = 0.615$, $T = 0.62$ (descending monotonically), taken from the full numerical solution at $Ra = 10^7$, $\varepsilon = 0.065$, $\mu = 1$, with $a = 3$ (so the cell is of width 3ε in x). Note that only half of the lid, $1.5 < X < 3$, is shown. The dashed isotherm for $T = 0.615$ is our preferred contour of the lid base.

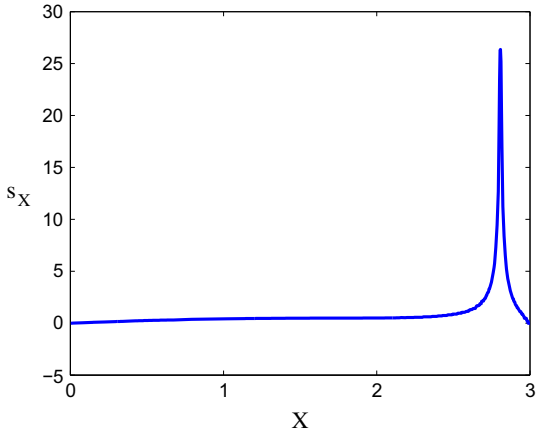

Figure 6. Slope of the $T = 0.615$ isotherm derived from the computed solution plotted in figure 5.

3.5.1. Boundary conditions

The problem arises through the specification of the boundary conditions for s. Insofar as we *define* the lid base $Z = s(X)$ by the isotherm $T = T_a$, the boundary conditions for s are that $s_X = 0$ at $X = 0$ and $X = a$, since $\theta_X = 0$ there. The question then arises as to which isotherm to use in practice. Figure 5 shows a sequence of isotherms within the asthenosphere, taken from the computation of the steady state solution of (11) with (12), using parameter values $a = 3$, $\varepsilon = 0.065$, $\mu = 1$, $Ra = 10^7$, which nicely delineate the formation of a weak plume at the right margin. Particularly, the choice of $T = 0.615$ as defining the lid base is actually exactly that defined by (23), and seems an apt choice.

Since $\chi = 0$ at $X = 0$, we automatically have $D = 0$ and thus $s_X = 0$ at $X = 0$. Note that, because the function $w/(1 + w^2)^2$ has a maximum at $w = 1/\sqrt{3}$, and since $s_X = 0$ at $X = 0$, the value of s_X in (41) that we require (for given D and s, two are possible) is that

Downloaded by [89.234.79.13] at 03:45 10 March 2016

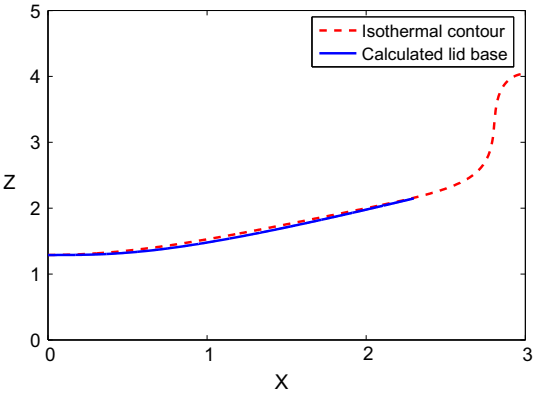

Figure 7. Comparison of the solution of (45) (solid (blue online) curve) with the full numerical dashed (red online) isotherm $T = 0.615$, using the value of $\nu = 0.284$ such that $s_X(0) = 0$, $s(0) = 1.29$ is the numerically computed value, and $s_X(2.3) = 1/\sqrt{3}$; $X = 2.3$ is the value where the numerically computed slope reaches the critical value $1/\sqrt{3}$.

to the left of the maximum, at least for small X, i.e. $s_X < 1/\sqrt{3}$, $\phi < \pi/6$. Similarly, the prescription of $s_X = 0$ at $X = a$ follows from $(37)_5$, since $\chi_Z = 0$ at $X = a$. However, this leads to an inconsistency in (41). A local expansion of χ near the corner indicates that if $s_X = 0$ at $X = a$, then

$$\chi \sim 1 - \alpha(a - X) \quad \text{near} \quad X = a, \quad Z = s, \tag{43}$$

so that $\chi_X \neq 0$ at $X = a$. In consequence, $D \neq 0$ in (42), and thus (41) implies $s_X \neq 0$ at $X = a$. The coupled problem as stated has no solution satisfying $s_X = 0$ at $X = a$.

However, matters are no better if we suppose $s_X \neq 0$ at $X = a$, as a local expansion for χ then implies

$$\chi \sim 1 - \alpha r^q \sin q\lambda, \tag{44}$$

where $a - X = r \sin\lambda$, and if $s_X = \tan\phi$, then $q = \pi/(\pi - 2\phi) > 1$, and in particular, $\chi_X = 0$ at $X = a$. This is consistent with (37), but again, not with (41). There is apparently no solution of the combined system (37) and (41) in which the slope of s is finite, and the only way in which the system can be solved is by supposing that $s_X \to \infty$ (thus effectively q is infinite in (44)), meaning $\chi_X \to 0$, and thus also D. This idea receives corroboration from the computed isotherm for $T = 0.615$, whose slope (thus s_X) is shown in figure 6. Apparently, a near blow-up occurs at $X \approx 2.8$. In more detail, examination of D suggests that it approaches zero at almost the same value, which is necessary in (41) if the slope is to become very large.

The resolution of this conundrum is the following. It is clear that prescription of $s_X = 0$ at $X = 0$ allows ψ and τ_3 defined in the asthenosphere by (29) to be zero, and also θ_X, using the definition of G in (40). However, use of (29) shows that $\psi = \mathrm{O}(1)$ as $X \to a$, and thus a boundary layer is necessary to accommodate the boundary condition for ψ (and also in fact τ_3 and θ). We discuss this *corner layer* below. For the moment, notice that it arises because (28) is a singular limit of (26), and thus the lid equation (32) and hence

Downloaded by [89.234.79.13] at 03:45 10 March 2016

(41) should be also. Thus we presume that the appropriate condition for (41) is a matching condition of some type, but it remains unclear if this is the case.

Further discussion is provided in Appendix A. In essence, we seek a (small) correction to (41) which is consistent with the behaviour indicated in figure 6. There is no unique way to do this, but without such a discussion, it is not clear what boundary condition to apply to (41). Figure 7 shows the solution of the modified equation

$$\nu s_{XX} + \frac{s_X}{(1+s_X^2)^2}\exp\left(\frac{-\mu s}{T_a}\right) = \beta D, \tag{45}$$

where the boundary conditions are taken to be $s_X(0) = 0$, $s_X(2.3) = 1/\sqrt{3}$, where we have used the value $X = 2.3$ where the computational solution takes this (critical) value of the slope, and we have chosen the value of $\nu = 0.284$ so that $s(0) = 1.29$, which is the computed value. This procedure is not ideal, but is at least self-consistent. In this way we avoid the inevitable awkwardness associated with the corner boundary layers, which are not in fact described by (45) (see Appendix A). Figure 7 shows that the agreement of this procedure with the actual position of the isotherm is very good.

3.6. Corner layer

We return to the asthenosphere equations (26). It is straightforward to see that the appropriate rescaling required for X in the corner layer in order to bring ψ down to zero is to put

$$Z = s(a) + \varepsilon\zeta, \qquad X = a - \varepsilon Y, \tag{46}$$

and the equations reduce to the full Stokes equations in the form

$$\begin{aligned} p_Y &= \tau_{1Y} + \tau_{3\zeta}, & p_\zeta &= \tau_{3Y} - \tau_{1\zeta} - \theta, \\ \tau_1 &= -2\eta\psi_{Y\zeta}, & \tau_3 &= \eta(\psi_{YY} - \psi_{\zeta\zeta}), \end{aligned} \tag{47}$$

and η is given by

$$\eta \approx \exp\left[-\frac{\theta}{T_a^2} + \frac{\mu s(a)}{T_a}\right]. \tag{48}$$

The scaled temperature is determined by

$$\psi_Y\theta_\zeta - \psi_\zeta\theta_Y = \varepsilon\nabla^2\theta; \tag{49}$$

thus $\theta \approx \theta(\psi)$, and the temperature is advected round the corner. The solution of (47) enables the passage of ψ and τ_3 to zero at the boundary, but the zero heat flux condition cannot be satisfied, since $\theta_Y \approx \theta'(\psi)\psi_Y \neq 0$ at $Y = 0$.

3.6.1. Corner plume

There is thus a further layer, which is a weak thermal plume, in which

$$Y = \varepsilon^{1/2}\tilde{Y}, \qquad \psi \sim \varepsilon^{1/2}v_p(\zeta)\tilde{Y}, \tag{50}$$

Downloaded by [89.234.79.13] at 03:45 10 March 2016

v_p is the downwards side wall velocity determined from the corner layer solution, and θ satisfies the approximate equation

$$v_p\theta_\zeta - v_p'\tilde{Y}\theta_{\tilde{Y}} = \theta_{\tilde{Y}\tilde{Y}}, \tag{51}$$

and this enables the satisfaction of the thermal boundary condition.

3.7. Upper core

Emerging downwards from the asthenosphere, $f \sim \zeta$, where f is the normalised stream function defined in (29), and it follows that we should rescale $\psi \sim 1/\varepsilon$, and hence also $p, \tau_1, \tau_3 \sim \varepsilon$. In terms of the variables in (11), this suggests

$$\tau_1,\ \tau_3,\ p \sim \varepsilon^4 Ra, \qquad \psi \sim \frac{1}{\varepsilon^2}, \qquad T = T_a + \varepsilon\theta, \qquad \eta \sim \eta_a, \tag{52}$$

whence the governing equations are those of Stokes flow with a variable viscosity,

$$\begin{aligned} p_X &= \tau_{1X} - \tau_{3Z}, & -p_Z &= \tau_{3X} + \tau_{1Z} + \frac{\theta}{\varepsilon^2},\\ \tau_1 &= 2\eta\psi_{XZ}, & \tau_3 &= \eta(\psi_{XX} - \psi_{ZZ}),\\ & & \varepsilon^2\theta_t + \psi_Z\theta_X - \psi_X\theta_Z &= \varepsilon^2\nabla^2\theta,\\ \eta &= \exp\left[\frac{\mu Z}{T} + \frac{1}{\varepsilon}\left(\frac{1}{T} - \frac{1}{T_a}\right)\right] \approx \exp\left[\frac{\mu Z}{T_a} - \frac{\theta}{T_a^2}\right]. \end{aligned} \tag{53}$$

We use this scaled set of equations as the basic reference set henceforth. In conventional boundary layer theory for temperature-dependent viscous convection, $\theta = 0$ to all orders of ε, and the same is true here. The reason for this is essentially the same as in the application of the Prandtl–Batchelor theorem, where the closed streamlines force a constant temperature in a steady flow (cf. Fowler 1985b). Although figure 4 suggests that at least some of the streamlines invade the lower core (and thus are not closed within the upper core), these are for low values of ψ, and the streamlines having $\psi \sim \mathrm{O}(1)$ are closed. Taking $\theta = 0$ to all orders of ε, the model reduces to a modified Stokes flow:

$$\begin{aligned} p_X &= \tau_{1X} - \tau_{3Z}, & -p_Z &= \tau_{3X} + \tau_{1Z},\\ \tau_1 &= 2\eta\psi_{XZ}, & \tau_3 &= \eta(\psi_{XX} - \psi_{ZZ}),\\ & & \eta &= \exp\left[\frac{\mu Z}{T_a}\right]. \end{aligned} \tag{54}$$

3.8. Lower core

In the lower core, which is also the lower mantle, we firstly rescale the upper core vertical coordinate Z as

$$z = 1 - \varepsilon Z. \tag{55}$$

We then choose a balance of terms in which thermal advection balances conduction and buoyancy balances shear stress, which itself balances shear strain rate. This scaling is based

Downloaded by [89.234.79.13] at 03:45 10 March 2016

on the apparent computational observation that there is no identifiable plume in the lower core. In retrospect, we shall find that in fact there is a mild plume of thickness $O(\varepsilon^{1/2})$, and this in manifested in figure 4, for example, by the mild clustering of streamlines at the left hand side. However, it is convenient to proceed as we do, since our analysis encompasses this possibility, and the plume is rather weak ($\varepsilon^{1/2} \approx 0.25$ for $\varepsilon = 0.065$). Note, however, that a consequence of (91), (78) and (66) below is that strictly speaking $\psi \sim \varepsilon^{3/2}$, rather than the choice in (56), and other scales are affected similarly. There is no consequent effect on our analysis, however.

This leads to the lower core rescaling (from (53))

$$\begin{aligned} p &\sim \frac{1}{\varepsilon^4}, \qquad \tau_1 \sim \frac{1}{\varepsilon}, \qquad \tau_3 \sim \frac{1}{\varepsilon^2}, \\ \psi &\sim \varepsilon^2, \qquad \eta \sim \eta_L = \frac{1}{\varepsilon^4}, \end{aligned} \tag{56}$$

and we define (the rescaled)

$$\eta = \mathrm{e}^{-\Theta}; \tag{57}$$

some algebra then shows from (53) that if in addition we define

$$T_L(z) = \frac{1+\mu(1-z)}{S_L}, \qquad S_L = \frac{1}{T_a} + \varepsilon \ln \eta_L, \tag{58}$$

then exactly

$$\Theta = \frac{S_L}{\varepsilon}\left(1 - \frac{T_L}{T}\right), \tag{59}$$

and to leading order we have

$$T \approx T_L + \frac{\varepsilon T_L \Theta}{S_L}. \tag{60}$$

Note that $T_L(z)$ is an isoviscous temperature profile.

Substituting the scalings (55), (56) and (60) into (53), we obtain the rescaled lower core equations

$$\begin{aligned} p_X &= \varepsilon^3(\tau_{1X} + \tau_{3z}), \qquad \frac{1}{\varepsilon}\{p_z - (T_L - T_a)\} = \tau_{3X} - \varepsilon^2\tau_{1z} + \frac{T_L\Theta}{S_L}, \\ \tau_1 &= -2\eta\psi_{Xz}, \qquad \tau_3 = \eta(\psi_{XX} - \varepsilon^2\psi_{zz}), \\ &\frac{T_L\Theta_t}{S_L} + \psi_X\left(1 + \frac{\varepsilon\Theta}{S_L}\right)T_L' + \frac{\varepsilon T_L}{S_L}(\psi_X\Theta_z - \psi_z\Theta_X) + \cdots \\ &\qquad = \frac{T_L\Theta_{XX}}{S_L} + \frac{\varepsilon^2}{S_L}\left[2T_L'\Theta_z + T_L\Theta_{zz}\right] + \cdots, \\ &\qquad \eta = \mathrm{e}^{-\Theta}, \end{aligned} \tag{61}$$

Downloaded by [89.234.79.13] at 03:45 10 March 2016

and here we retain the time derivative for the moment. At leading order we thus have the system

$$\begin{aligned} p &= p(z), & p' &= T_L - T_a + \varepsilon \Pi'(z), \\ \tau_{3X} &= -\frac{T_L \Theta}{S_L} + \Pi'(z), & \tau_3 &= \psi_{XX} \mathrm{e}^{-\Theta}, \\ & \frac{T_L \Theta_t}{S_L} + \psi_X T_L' = \frac{T_L \Theta_{XX}}{S_L}, \end{aligned} \tag{62}$$

where $\Pi(z)$ is to be determined. The equations (62) are subject to the boundary conditions

$$\Theta_X = \tau_3 = \psi = 0 \qquad \text{on} \qquad X = 0,\ a. \tag{63}$$

Solving these, we have

$$\tau_3 = -\frac{T_L}{S_L} \int_0^X \Theta \, \mathrm{d}X + \Pi' X, \tag{64}$$

whence

$$\Pi' = \frac{T_L}{a S_L} \int_0^a \Theta \, \mathrm{d}X, \tag{65}$$

and if we write

$$W = \frac{\mu \psi_X}{T_L}, \tag{66}$$

(noting that $T_L' = -\mu / S_L$), then Θ and W satisfy the coupled equations

$$\Theta_t = \Theta_{XX} + W, \qquad \left[\mathrm{e}^{-\Theta} W_X \right]_X = -\frac{\mu}{S_L} \left(\Theta - \frac{1}{a} \int_0^a \Theta \, \mathrm{d}X \right), \tag{67}$$

subject to

$$\Theta_X = W_X = 0 \qquad \text{on} \qquad X = 0,\ a. \tag{68}$$

All the boundary conditions are satisfied at the side, as in effect the basal plume occupies the entire width of the cell.

We now consider steady state solutions of this system. Eliminating W, we have

$$\left[\Theta_{XXX} \mathrm{e}^{-\Theta} \right]_X = \frac{\mu}{S_L} \left(\Theta - \frac{1}{a} \int_0^a \Theta \, \mathrm{d}X \right), \tag{69}$$

with the boundary conditions

$$\Theta_X = \Theta_{XXX} = 0 \qquad \text{on} \qquad X = 0,\ a. \tag{70}$$

To solve this, we define

$$m(z) = \frac{1}{a} \int_0^a \Theta \, \mathrm{d}X, \tag{71}$$

and we write

$$\Theta = m(z) + \Phi, \qquad X = ay, \tag{72}$$

so that Φ satisfies

Downloaded by [89.234.79.13] at 03:45 10 March 2016

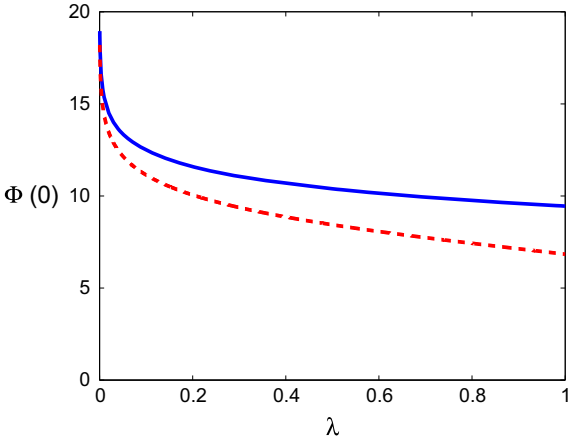

Figure 8. The variation of $\Phi(0)$ with λ (upper curve). Also shown is the asymptotic result for small λ, (87) (dashed).

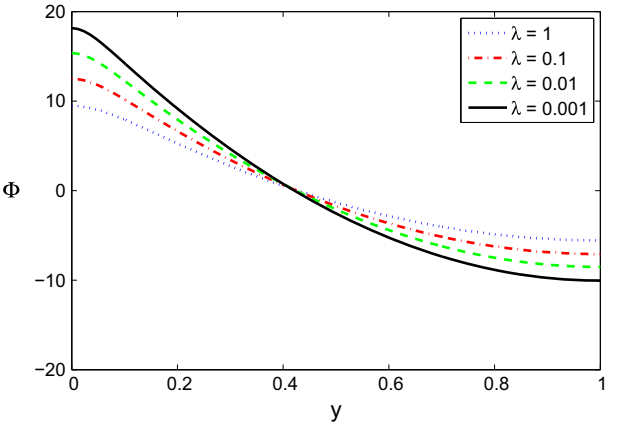

Figure 9. Solutions of (73) with (75) for various values of λ.

$$\left[\Phi_{yyy}\mathrm{e}^{-\Phi}\right]_y = \lambda\Phi, \tag{73}$$

where

$$\lambda = \frac{\mu a^4 \mathrm{e}^m}{S_L}, \tag{74}$$

and

$$\Phi_y = \Phi_{yyy} = 0 \qquad \text{on} \qquad y = 0,\ 1. \tag{75}$$

Note that

$$\int_0^1 \Phi \, \mathrm{d}y = 0. \tag{76}$$

Figure 8 shows the variation of the maximum $\Phi(0)$ with λ, obtained by numerical solution of the boundary value problem (73) with (75), and figure 9 shows the solution of (73) for various values of λ. Figure 8 is consistent with the fact that the steady solution emerges from $\Phi = 0$ at $\lambda = \pi^4$ in a sub-critical pitchfork bifurcation, and is actually

Downloaded by [89.234.79.13] at 03:45 10 March 2016

unstable, as is easily ascertained by a weakly nonlinear analysis near $\lambda = \pi^4$. Despite this, the steady solution shows good agreement with the full numerical solution. We comment further on this in the conclusions. As can be seen in figure 8, $\Phi(0)$ becomes large as $\lambda \to 0$, and figure 9 shows a sequence of solutions at small λ, whose asymptotic form is described as follows.

We define the large parameter Λ ($\approx \Phi(0)$) via

$$\lambda = \Lambda^3 \mathrm{e}^{-\Lambda}, \tag{77}$$

so that $\Lambda \sim \ln 1/\lambda$. There is an outer solution where $y \sim \mathrm{O}(1)$ and we put

$$\Phi = \Lambda\phi\,; \tag{78}$$

then, assuming $\phi < 1$, we have that $\phi''' = 0$ correct to exponentially small terms in Λ, so that

$$\phi \approx 1 - 3y + \tfrac{3}{2}y^2, \tag{79}$$

which satisfies the boundary conditions at $y = 1$ and also the integral constraint (76). Note that the outer solution is zero at $y = 1 - (1/\sqrt{3}) \approx 0.42$ independently of λ, as can be seen in figure 9.

There is a boundary layer near $y = 0$ where the slope adjusts to zero. We put

$$y = \frac{Y}{\Lambda}, \qquad \Phi = \Lambda + \chi, \tag{80}$$

so that the matching condition to (79) is

$$\chi \sim -3Y \qquad \text{as} \qquad Y \to \infty. \tag{81}$$

At leading order, χ satisfies

$$\left[\mathrm{e}^{-\chi}\chi'''\right]' = 1, \tag{82}$$

and thus

$$\chi''' = Y\mathrm{e}^{\chi},$$

$$\chi'(0) = \chi'''(0) = 0, \qquad \chi'(\infty) = -3. \tag{83}$$

For this, we solve numerically the initial value problem

$$f'''(x) = x\mathrm{e}^{f},$$
$$f(0) = f'(0) = 0, \qquad f''(0) = -B, \tag{84}$$

and we choose the unique[3] value of B such that $f''(\infty) = 0$; this value is $B \approx 1.14$, and the resulting value of

$$K = -f'(\infty) \approx 1.69. \tag{85}$$

[3] Uniqueness follows from a comparison argument.

Downloaded by [89.234.79.13] at 03:45 10 March 2016

The solution of (83) is then

$$\chi = 4\ln\frac{3}{K} + f\left(\frac{3Y}{K}\right); \tag{86}$$

in particular,

$$\Phi(0) = \Lambda + \chi(0) \approx \Lambda + 2.3. \tag{87}$$

To complete the lower core solution, we need to choose the value of $m(z)$ in (71). Equivalently, we need to choose the value of λ in (74). To do this, we use the exact integral constraint from (15) and (20), which implies

$$\begin{aligned}\int_0^a (T\psi_X + T_Z)\,\mathrm{d}X &\approx \varepsilon\int_0^a \left(\frac{T_L}{S_L}\Theta\psi_X - T_L'\right)\mathrm{d}X \\ &= (T_a - T_0)\int_0^a (1+s_X^2)G(X)\,\mathrm{d}X,\end{aligned} \tag{88}$$

and this reduces, using (36), (37), (39) and (40), to

$$\frac{T_L^2}{\mu S_L}\int_0^a \Phi_X^2\,\mathrm{d}X = \frac{C(T_a - T_0)}{\varepsilon} - \frac{\mu a}{S_L}, \tag{89}$$

where C is the lid constant given by (35).[4]

To calculate the integral, let us suppose that $\lambda \ll 1$. From (78) and (79), it follows that

$$\int_0^a \Phi_X^2\,\mathrm{d}X \approx \frac{3\Lambda^2}{a}, \tag{90}$$

and thus m is chosen in terms of the lid thickness s by requiring

$$\frac{3\Lambda^2 T_L^2}{a\mu S_L} = \frac{C(T_a - T_0)}{\varepsilon} - \frac{\mu a}{S_L}, \tag{91}$$

assuming $\lambda \ll 1$, which essentially requires $m < 0$. We see from this that $\Lambda \sim 1/\sqrt{\varepsilon}$, so that this assumption is justified. (See the comment following (55).)

We can compare these asymptotic temperature profiles with those computed from the full numerical simulation. In order to do this we need to estimate $m(z)$. In principle we can use (91), but this is somewhat circuitous, and it is more direct to use the full numerical solution in the lower mantle directly. Specifically, we have from (71), (58) and (59) that

$$\Phi(0) - \Phi(1) = \frac{1+\mu(1-z)}{\varepsilon}\left(\frac{1}{T_+} - \frac{1}{T_-}\right), \tag{92}$$

where T_+ and T_- are the dimensionless temperatures at $y = 1$ and $y = 0$, respectively. Since the left hand side is an increasing function of λ, we can use the computed values of $T_\pm$ to determine λ, and hence (from (74)) m, assuming (from (58) and (23))

$$S_L = 1 + \mu + \varepsilon\ln\left(\varepsilon^4 Ra\right). \tag{93}$$

[4]Note that from (15), $Nu = C(T_a - T_0)/\{\varepsilon a(1 - T_0)\}$.

Downloaded by [89.234.79.13] at 03:45 10 March 2016

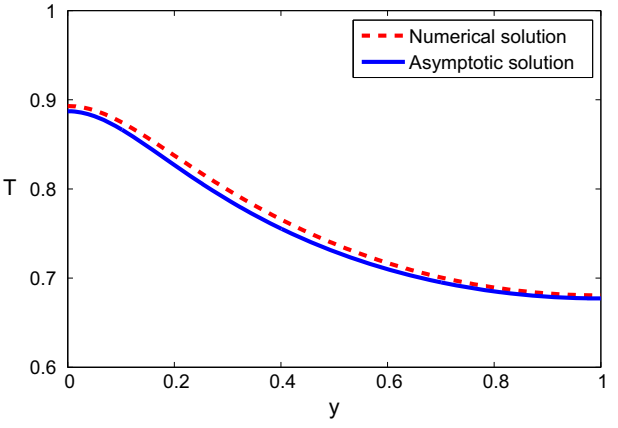

Figure 10. Comparison of full numerical and asymptotic solutions for lower mantle temperature T as a function of y, at $z = 0.2$. Details are described in the text.

Downloaded by [89.234.79.13] at 03:45 10 March 2016

Equations (59) and (72) then determine T, and as can be seen in figure 10, the agreement is very good.

An alternative procedure for determining S_L directly rather than using (93) is to note that

$$m = \frac{1}{\varepsilon}\left[S_L - \{1 + \mu(1-z)\}\left(\overline{\frac{1}{T}}\right)\right], \tag{94}$$

where the overbar denotes the horizontal average, and hence

$$\Phi(0) = \frac{1+\mu(1-z)}{\varepsilon}\left[\left(\overline{\frac{1}{T}}\right) - \frac{1}{T_-}\right], \qquad \Phi(1) = \frac{1+\mu(1-z)}{\varepsilon}\left[\left(\overline{\frac{1}{T}}\right) - \frac{1}{T_+}\right]; \tag{95}$$

either can be used to estimate λ and thus m, and then (94) gives an estimate for S_L in each case; in practice we take the average of the two estimates.

3.9. Basal thermal boundary layer

The solutions of the lower core equations (61) satisfy all the boundary conditions at the sides, but they do not satisfy the basal boundary conditions, which are of the form (in terms of the lower core scaled variables)

$$\tau_3 = \psi = 0, \qquad \Theta = \Theta_b \equiv \ln\left(\varepsilon^4 Ra\right) \qquad \text{at} \qquad z = 0, \tag{96}$$

where we have used the definition of T_a in (23), and (56), (58) and (59), together with the basal condition $T = 1$ at $z = 0$. The lower core equations are given by (61), and the basal thermal boundary layer equations are obtained by writing

$$z = \varepsilon Z, \qquad \tau_1 \sim \frac{1}{\varepsilon}, \qquad p = \int_0^z (T_L - T_a)\,\mathrm{d}z + \varepsilon^2 P, \tag{97}$$

which yields the rescaled equations, to leading order,

$$\begin{aligned} P_X &= \tau_{1X} + \tau_{3Z}, & P_Z &= \tau_{3X} - \tau_{1Z} + \frac{T_L\Theta}{S_L}, \\ \tau_1 &= -2\,\eta\psi_{XZ}, & \tau_3 &= \eta(\psi_{XX} - \psi_{ZZ}), \\ -\mu\psi_X + T_L(\psi_X\Theta_Z - \psi_Z\Theta_X) &= T_L\nabla^2\Theta, \\ \eta &= \mathrm{e}^{-\Theta}, \end{aligned} \tag{98}$$

wherein we can take

$$T_L \approx T_L(0) = \frac{1+\mu}{S_L}. \tag{99}$$

Again, we have the full Stokes equations. The solutions must satisfy the basal boundary conditions (96), the sidewall boundary conditions (63), and the matching conditions as $Z \to \infty$ in which Θ, τ_3 and ψ tend to the limits given by (64) and (69).

There seems to be some mild scope for further approximation, since the basal value of Θ in (96) is "large" if $Ra \gg \varepsilon^{-4}$. In practice, there is little to be gained, since apparently computation of the basal boundary layer is not necessary for the determination of the rest of the solution, and in any case Θ_b is not typically that large. For our typical values of $\varepsilon = 0.065$ and $Ra = 10^7$, we have $\Theta_b \approx 5.2$, although the basal viscosity does then drop to 0.56×10^{-2} relative to the lower core, as can be seen in figure 3.

Note that integration of the energy equation over the flow domain yields the Nusselt number relation

$$-\int_0^a \left.\frac{\partial\Theta}{\partial Z}\right|_{Z=0} \mathrm{d}X = \frac{T_L}{\mu}\int_0^a \Theta_\infty'^2\,\mathrm{d}X, \tag{100}$$

where $\Theta_\infty(X)$ is the solution of (69) and (70).

3.10. Transition zone

It is fairly clear that a transition zone between the upper and lower core is necessary, since the variables, and specifically the temperature, do not match. Because the viscosity increases exponentially with depth, the stream function in the upper core tends exponentially (and fairly rapidly) to zero, but the approximations involved in the upper core, specifically the loss of the conduction term, become invalid when $\psi \sim \varepsilon^2$, and this heralds the occurrence of a transition zone. Just as in the lower core, this occurs when $\eta \sim \eta_L = 1/\varepsilon^4$, but since $\eta = \exp\left(\mu Z/T_a\right)$ in the upper core, this tells us that the transition region is accessed by rescaling Z as

$$Z = Z_L + Y, \qquad Z_L = \frac{T_a}{\mu}\ln\left(\frac{1}{\varepsilon^4}\right), \tag{101}$$

and the other variables are rescaled as

$$p \sim \tau_1 \sim \tau_3 \sim \frac{1}{\varepsilon^2}, \qquad \psi \sim \varepsilon^2, \qquad \eta \sim \frac{1}{\varepsilon^4}. \tag{102}$$

Note that for the computations in figures 2–4, $Z_L = 6.72$, corresponding to $z = 0.56$.

Downloaded by [89.234.79.13] at 03:45 10 March 2016

L: lid (lithosphere)

A: asthenosphere

UM: upper mantle circulation

LM: lower mantle return flow

BL: core–mantle thermal boundary layer

Figure 11. The principal regions of the convection cell structure, shown with two actual streamlines of the convective flow shown in figure 4, with the appropriate aspect ratio.

Downloaded by [89.234.79.13] at 03:45 10 March 2016

Substituting these new scales into (53), we find

$$\begin{aligned} p_X &= \tau_{1X} - \tau_{3Y}, \qquad -p_Y = \tau_{3X} + \tau_{1Y} + \theta, \\ \tau_1 &= 2\eta\psi_{XY}, \qquad \tau_3 = \eta(\psi_{XX} - \psi_{YY}), \\ \psi_Y\theta_X - \psi_X\theta_Y &= \nabla^2\theta, \\ \eta &= \mathrm{e}^{-\Theta}, \end{aligned} \tag{103}$$

and the relation of θ and Θ is given approximately by

$$\theta \approx \mu T_a Y + T_a^2\Theta. \tag{104}$$

The equations (103) are the full Stokes equations, together with the full temperature equation. Of principal interest is the transition in the temperature, where apparent matching conditions should be

$$\begin{aligned} \theta &\to 0 \qquad \text{as} \qquad Y \to -\infty, \\ \theta &\sim \mu T_a Y + T_a^2\Theta_1(X) \qquad \text{as} \qquad Y \to \infty, \end{aligned} \tag{105}$$

where $\Theta_1(X)$ is the value of Θ in the lower core when $z \to 1$. An Oseen-like simplification comes from the fact that (since $S_L \approx 1/T_a$) $\psi \approx -(1/\mu T_a)\theta_X$ in the lower core (and is independent of Y as $z \to 1$). If we use this for the vertical advection term, then the equation for θ is simply

$$\left[1 - \frac{\theta_Y}{\mu T_a}\right]\theta_{XX} + \theta_{YY} = 0, \tag{106}$$

together with the matching conditions in (105), and a solution of this seems feasible.

Figure 11 shows a cartoon of the principal regions of the convective structure of the cell, for an approximately one to five aspect ratio cell, such as we have used in our illustrations here. Below the stagnant lid, the asthenosphere is a relatively rapid shear flow which drives

an approximately isothermal circulation in the upper mantle, also called the upper core. The lower mantle or lower core below this is an approximately vertical return flow in which there is a mild excess of buoyancy in an upwelling plume. The basal boundary layer is only thin relative to the total depth; it is comparable in thickness to the width of the cell. Other regions we have alluded to are not depicted here, notably corner layers at each end of the asthenosphere, and a transition zone between upper and lower mantle.

4. Discussion

In this discussion, we summarise what we have done and what we have not yet done, and we comment on extensions of the model to make it more sensibly relevant to the Earth's mantle; in the conclusions we will discuss the possible relevance of these results for convection in the mantle of terrestrial planets.

We believe that we have essentially solved the problem of elucidating the asymptotic structure of high Rayleigh number convection in a fluid whose viscosity depends exponentially strongly on both temperature and pressure. There are two central obstacles to establishing the results. The first is practical: computations with viscosity contrasts even as large as 10^{15} fail to portray an obvious asymptotic structure, and previous computational work has failed to progress beyond this. The second obstacle is the fundamental issue of how a rapidly convecting thermobaroviscous fluid reconciles its tendency to be isothermal (or more generally, adiabatic) with the necessity to be relatively isoviscous[5] (below the rigid lid). Fowler (1983) suggested that a relatively isoviscous lower mantle could satisfy constraints associated with dynamics, mantle viscosity estimates, core mantle temperature estimates, as well as a low viscosity asthenosphere, a vigorous upper mantle flow and a sluggish lower mantle flow, but he was unable to substantiate these claims by means of an actual solution.

As we now see, this inability is largely due to the inability to recognise that the way the flow copes with the necessity to be relatively isoviscous in the lower mantle is by adopting the form of narrow convection cells. This revelation, due to Khaleque (2015) and expounded by Khaleque *et al.* (2015), allowed us to push the computed results to extreme viscosity contrasts and thereby identify the appropriate asymptotic limits. Even with this insight, however, the unravelling of the flow structure has been a laborious process.

Figure 12 shows the mid-cell vertical temperature profile from the full numerical solution, and it can be compared to figure 2 of Fowler (1983), for example. The main difference between the solution structure suggested there and that found here is that slightly larger variations in viscosity are admitted in the asymptotic solution. For example, the jump ΔT of temperature in the basal boundary layer of figure 12 corresponds to a dimensional jump of about 700 K, while Fowler's 1983 order of magnitude suggestion was $\Delta T \sim \varepsilon$, corresponding to a dimensional jump $\sim \varepsilon T_b \sim 230$ K for the values we use here; associated with the 700 K jump is a viscosity decrease (see figure 3) of some two to three orders of magnitude. The actual value is larger than the earlier estimate because of the basal thermal boundary condition in (96) involving $\ln(\varepsilon^4 Ra)$. Interestingly, this relatively large jump is similar to that found by Loper (1985), whose work remarkably described mantle convection as a finger-like flow (in the sense of being essentially a vertical exchange

[5] By relatively isoviscous, we mean to allow variations of perhaps five orders of magnitude, but not 20.

Downloaded by [89.234.79.13] at 03:45 10 March 2016

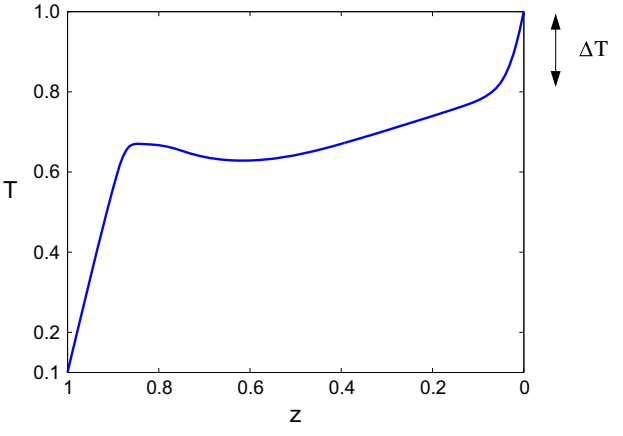

Figure 12. The mid-cell temperature at $X = \frac{1}{2}a$ as a function of z (note that the profile is from the surface towards the base). This is taken from the full numerical solution with $a = 3$, $\varepsilon = 0.065$, $Ra = 10^7$, $\mu = 1$.

Downloaded by [89.234.79.13] at 03:45 10 March 2016

flow). Loper (1985) also asserted the tendency of the medium to become isoviscous. It seems unlikely that such a large temperature jump could be supported unless the cells are narrow. To put it the other way round, one expects such a high temperature jump to be very unstable, and thus to cause the width of convective boundary layers to be narrow.

Our analysis shows that the convective structure consists of a stagnant lid, and a relatively fast shearing return flow in the upper mantle beneath the lid, whose velocities for the parameters in figure 4 are of order $3\,\mathrm{mm\,y^{-1}}$; obviously less than plate tectonic velocities on Earth, but we are not describing the oceanic subduction-driven plate motion. In the lower mantle there is an essentially vertical return flow with downwards velocities of order $0.8\,\mathrm{mm\,y^{-1}}$, and upwards ("plume") velocities of the order of $4\,\mathrm{mm\,y^{-1}}$, which accelerate in the upper mantle (see figure 4). The relative sluggishness of the lower mantle apparent in figure 4 is a consequence of the tallness of the convective cells.

In the stagnant lid, the viscosity is enormous, but below this, there is a pronounced structure. The lowest viscosity is in the upper mantle (down to a dimensional depth of about 900 km), where it is about two orders of magnitude lower than the basal viscosity, and then it is higher in the lower mantle, ranging horizontally from the basal viscosity to a value about four orders of magnitude higher. Supposing as we expect that it is the lower viscosity material which controls short term post-glacial rebound, for example, these results appear to be consistent with inferred estimates of mantle viscosity.

The temperature shown in figures 2 or 12, for example, is distinctly non-isothermal below the rigid conductive lid. There is a relatively small isothermal upper core down (in figure 12) to about $z = 0.8$, and below this a transition zone in which the temperature drops, before reaching a profile in the lower mantle which increases linearly with depth; however, the slope in figure 12 is 0.35, whereas an isoviscous gradient would be a touch under 0.5. The difference is not large, but enough to cause several orders of magnitude change in viscosity.

Our principal comparison of the theory with the numerical computation is in the determination of the lower mantle temperature profile and the position of the base of the

lithospheric lid. Both of these are excellent, but our analysis of the lid base is certainly one that warrants further technical examination; and indeed, there are a number of other lines of enquiry which could be pursued. We have delineated approximating equations in numerous areas (for example, the upper core, the basal boundary layer) without attempting to provide a numerical solution. Largely this is because such investigations do not add significant information to our study, which is already a long one. We think that the most significant point worthy of further study is the issue of the lid base equation. In particular, we note that the treatment of the lid base for thermoviscous convection (Fowler 1985a) was over-simplified, and itself deserves further study. Crucial in our analysis is the idea that the lid base is self-determining without reference to the flow elsewhere, and this is in stark contrast to the constant viscosity flow (Roberts 1979). In the thermoviscous case, the lid thickness (the parameter γ in (16)) was determined by the connection of the buoyant plume to the asthenospheric shear flow, but in the present case, the buoyancy of the plume is insignificant in the upper core and the upper core flow is driven by the asthenospheric shear flow, which itself is driven by the lid slope.

Downloaded by [89.234.79.13] at 03:45 10 March 2016

4.1. Adiabatic and internal heating

In our analysis, we have assumed certain parameters to be constant, whereas in reality they will vary, particularly with pressure and thus depth. We took the dissipation number D in (1) to be zero, whereas its value is about 1.0 near the surface, and decreases to about 0.2 near the CMB (Ricard 2009), and we neglected internal heating, H. The value of this is uncertain, but various estimates suggest a value of $H \approx 4 \times 10^{-12}\,\mathrm{W\,kg^{-1}}$, which if distributed throughout the mantle would produce about half the observed oceanic heat flux (Jaupart *et al.* 2009).

If we include these two terms in the heat equation, then the original dimensional equation

$$\rho_m c_p \frac{\mathrm{d}T}{\mathrm{d}t} - \alpha T \frac{\mathrm{d}p}{\mathrm{d}t} = k\nabla^2 T + \rho H \tag{107}$$

becomes when non-dimensionalised as in (6) (we omit the time derivative),

$$\psi_x (T_z - T'_{\mathrm{ad}}) - \psi_z T_x = \nabla^2 T + Q, \tag{108}$$

where we may take the adiabatic temperature

$$T_{\mathrm{ad}} \approx T_a \exp\left[\int_z^1 D\,\mathrm{d}z\right], \tag{109}$$

and the dimensionless heating is

$$Q = \frac{\rho_m H d^2}{k T_b}, \tag{110}$$

in which k is the thermal conductivity, ρ_m is the mantle density. Taking values $\rho_m = 4 \times 10^3\,\mathrm{kg\,m^{-3}}$, $k = 4\,\mathrm{W\,m^{-1}\,K^{-1}}$, $d = 3000\,\mathrm{km}$, $H = 4 \times 10^{-12}\,\mathrm{W\,kg^{-1}}$, $T_b = 4000\,\mathrm{K}$ (Jaupart *et al.* 2009), we get $Q \approx 9$, and we write

$$Q = \frac{q}{\varepsilon}, \tag{111}$$

where for a value of $\varepsilon = 0.055$, we would have $q \approx 0.5$, so we take $q = \mathrm{O}(1)$.

Now we wish to see what the form of the scaled heat equation becomes in the upper core and lower core. In the upper core, we proceed first via (10), and then via (52), to obtain

$$\psi_Z \theta_X - \psi_X(\theta_Z - DT_a) = \varepsilon^2(\nabla^2\theta + q). \tag{112}$$

The effect of heating is to cause the upper core to be non-isothermal but the potential temperature $\theta - DT_aZ$ is constant on (closed) streamlines, and the heat generated leaks out conductively, as explained by Fowler (1985b).

In the lower core, we proceed from (53) via (55), (56) and (60), and find that the leading order terms are (in the steady state)

$$(T_L' - T_{\mathrm{ad}}')\psi_X = q + \frac{T_L}{S_L}\Theta_{XX}. \tag{113}$$

Now there is a divergence. If $q \neq 0$, integration of (113) from $X = 0$ to $X = a$ shows that not all the boundary conditions can be satisfied. Thus, although equation (113) is well scaled, it suggests that a boundary layer must exist, for which the best candidate may be a thermal plume. We will not pursue this here, other than suggesting that the presence of internal heating does not seem to have a major effect on our analytic description.

Downloaded by [89.234.79.13] at 03:45 10 March 2016

4.2. Activation enthalpy

In our analysis we took the activation energy E^* and the activation volume V^* to be constant, and in particular we used values appropriate for the deformation of olivine in the upper mantle (e.g. Karato and Wu 1993). It is difficult to assess appropriate values in the lower mantle, but a consensus has emerged which suggests that both E^* and V^* are lower (Yamazaki and Karato 2001, Ammann *et al.* 2009, 2010), as well as accommodating the accepted idea that V^* decreases with increasing depth (Sammis *et al.* 1977). Yamazaki and Karato suggest that the lack of seismic anisotropy in the lower mantle suggests that diffusion creep is the relevant creep process, for which estimates of the diffusion coefficients of for example oxygen and silicon in perovskite $MgSiO_3$ (Ammann *et al.* 2009) suggest that V^* is lower, around 2–3 $\mathrm{cm}^3\,\mathrm{mol}^{-1}$. More pertinently, estimates of consequent lower mantle viscosity profiles using assumed geotherms indicate that viscosity profiles are broadly consistent with direct inferences from post-glacial rebound and the like (e.g. Ammann *et al.* 2010), but Yamazaki and Karato warn that "this conclusion is highly dependent upon several poorly constrained mineral physics parameters".

Nevertheless, it is reasonable to suppose that the adiabatic profile T_{ad} in (109) and the isoviscous profile $T_L = [1 + \mu(1 - z)]/S_L$ are quite close. The issue is, are they *precisely* equal? This would be a remarkable coincidence, and if they are not precisely equal, then the lower core solution proceeds as before, with the modification that the lower core equation (69) is replaced by

$$\left[\Theta_{XXX}\mathrm{e}^{-\Theta}\right]_X = (T_{\mathrm{ad}}' - T_L')\left(\Theta - \frac{1}{a}\int_0^a \Theta\,\mathrm{d}X\right), \tag{114}$$

and the solution proceeds exactly as before providing the isoviscous profile is a steeper function of depth than the adiabatic profile, that is to say, the viscosity increases along an adiabat.

The crux of the matter is, what controls the aspect ratio? As Fowler (1983) pointed out, realistic parameter choices can easily be found consistent with a fairly uniform viscosity, but the cost is that the adiabatic temperature profile leads to an adiabatic temperature near the CMB which is low. Fowler estimated this to be 2330 K, and the estimate in figure 10 of Jaupart *et al.* (2009) is even lower, at 2200 K. The problem is that the CMB temperature is presently estimated to be ~ 4000 K (Jaupart *et al.* 2009), and the consequent estimated temperature jump at the boundary layer is further suggested by the post-perovskite phase change which is thought to occur at the CMB. Even if the activation enthalpy $H^* = E^* + pV^*$ at the CMB is as low as 500 kJ mol^{-1}, as suggested by Yamazaki and Karato (2001), a change of temperature from 2300 to 4000 K entails a viscosity jump of about 6.8×10^4. It is very difficult to imagine that such a jump can occur in an order one aspect ratio convection cell.

5. Conclusions

Our study has been motivated by convection in the Earth's mantle, but has been an idealised one, and has not been overly constrained by the detail that constitutes the reality of the problem. Despite this, the motivation impels us to consider whether what we have learned is likely to have any bearing on the real Earth, despite all the caveats discussed in the preceding section. Even if turns out to be irrelevant to the Earth, the theory may have implications for extra-solar "super-Earths", where larger values of mantle depths may lead to larger values of the viscous pressure number μ (Tackley *et al.* 2013).

Our principal finding is that at viscosity contrasts in excess of 10^{30}, narrow convection cells become the norm, and we have found an asymptotic structure which is consistent with this. The question is, how robust is this structure, and is it likely to occur in the real Earth, or indeed in other terrestrial planets? We have interpreted the tendency towards narrow cells as being indicative of the necessity for the interior viscosity to remain relatively uniform, but we might equally interpret it as a way in which the relatively high viscosity jump at the base can be stably maintained. It is certainly the case that in purely temperature-dependent viscous convection in O(1) aspect ratio cells, the basal temperature jump diminishes as the viscosity number ε decreases, and we associate this with increasing instability as the viscosity jump in the basal thermal boundary layer increases. The maximum jump that can be stably maintained in a square cell for thermobaroviscous convection appears to be about 10^3 (Khaleque 2015, figure 4.5). The notion that in the Earth there is a basal jump in excess of 10^4 is suggestive of the adoption of narrow cells.

Throughout our analysis, we have referred to the different parts of the flow by their geophysical counterparts, simply because there is a natural correspondence. There is a rigid lid, and this is the lithosphere. There is a low viscosity zone below this, which is the asthenosphere. The circulatory flow in the upper core corresponds to the upper mantle, while the more or less vertical exchange flow in the lower core corresponds to the lower mantle. One might even associate the core-mantle thermal boundary layer with the D″ layer, although it seems more likely that this is associated with other processes, including

Downloaded by [89.234.79.13] at 03:45 10 March 2016

for example the reaction between the outer core and the lower mantle (Knittle and Jeanloz 1991), and the post-perovskite transition alluded to above (Jaupart *et al.* 2009).

The main and obvious difference from the Earth's mantle is that there is no subduction. Various authors (Fowler, 1985a, 1993b, Tackley 1998, Tackley 2000a,b, Fowler and O'Brien 2003) have suggested that the weakening of the lithosphere necessary to initiate subduction is associated with viscoplastic yielding induced by the enormous stresses produced in the lithosphere, which are there essentially because they are necessary to support a heavy stagnant lithosphere. Numerical computations of lid stresses are rarely reported, unsurprisingly since the computations tend to exhibit instability, but they can be analysed asymptotically (Fowler 1985a), though we have not done so here; however, the analysis should be similar. Lid stresses become huge, and provide a mechanism for subduction.

The tantalising question is then, how should we expect convection to occur in a thermobaroviscous mantle when there is active subduction? For sub-continental lithosphere, we might expect the structure to be that described here. The most obvious distinction for oceanic lithosphere is that the plunge of the heavy lid causes a near horizontal return flow with a much larger horizontal length scale, but this will be restricted to the upper mantle; the lower mantle maintains its higher viscosity and sluggish convection. If we suppose that the lower mantle retains a finger-style convection, then it seems that leakage of upper mantle lithosphere to the lower mantle will occur locally, and most of the lower mantle may be effectively segregated from the upper mantle. But in any case, the residence time in the lower mantle for a $3\,\mathrm{mm\,y^{-1}}$ flow descending and then ascending a 2300 km deep finger cell is 1.5×10^9 y, and this seems to provide a robust way to segregate the mantle geochemically.

The issue of plume and mega-plume formation can not be readily addressed, as such features are essentially associated with time-dependent convection. Constant viscosity convection certainly becomes unstable and plume-like at high Rayleigh number, and it is interesting in this context to note that the lower mantle approximate model (67) has a steady solution which bifurcates unstably, as noted after (76). We have not found such instability in our numerical calculations, which suggests that a further stabilising bifurcation may occur at smaller λ. However it is tempting to suppose that if there is a real instability, the result could be plume formation on a horizontal scale comparable to the finger width, perhaps of order $l = 300\,\mathrm{km}$ (corresponding to $a = 1.8$, $\varepsilon = 0.055$, $d = 3000\,\mathrm{km}$). It is noteworthy that this scale is comparable to that of coronae on Venus, which may also represent the surface expression of mantle plumes (Solomatov and Head 1991). We might expect such plumes to punch their way through the upper mantle oceanic return flow. Their development time scale is $l^2/\kappa \sim 3000\,\mathrm{Ma}$, but a thermal runaway-type process could significantly reduce this. Even if there were many fingers, relatively few would provide plumes at any one time. It is less easy to see how mega-plumes might form, however, unless from a punch through of a subducting slab to the lower mantle and its subsequent foundering at the CMB.

Downloaded by [89.234.79.13] at 03:45 10 March 2016

Acknowledgements

T.S.K. acknowledges the award of a Felix scholarship from the University of Oxford. A.C.F. acknowledges the support of the Mathematics Applications Consortium for Science and Industry (www.macsi.ul.ie) funded by the Science Foundation Ireland [grant number 12/1A/1683].

Downloaded by [89.234.79.13] at 03:45 10 March 2016

Disclosure statement

No potential conflict of interest was reported by the authors.

References

Ammann, M.W., Brodholt, J.P. and Dobson, D.P., DFT study of migration enthalpies in $MgSiO_3$ perovskite. *Phys. Chem. Miner.* 2009, **36**, 151–158.

Ammann, M.W., Brodholt, J.P., Wookey, J. and Dobson, D.P., First-principles constraints on diffusion in lower-mantle minerals and a weak D″ layer. *Nature* 2010, **465**, 462–465.

Bercovici, D., A simple model of plate generation from mantle flow. *Geophys. J. Int.* 1993, **114**, 635–650.

Bercovici, D., The generation of plate tectonics from mantle convection. *Earth Planet. Sci. Lett.* 2003, **205**, 107–121.

Cathles, L.M., *The Viscosity of the Earth's Mantle*, 1975. (Princeton, NJ: Princeton University Press).

Christensen, U.R., Heat transport by variable viscosity convection and implications for the Earth's thermal evolution. *Phys. Earth Planet. Inter.* 1984a, **35**, 264–282.

Christensen, U.R., Convection with pressure- and temperature-dependent non-Newtonian rheology. *Geophys. J. R. Astron. Soc.* 1984b, **77**, 343–384.

Christensen, U.R., Heat transport by variable viscosity convection II: pressure influence, non-Newtonian rheology and decaying heat sources. *Phys. Earth Planet. Inter.* 1985, **37**, 183–205.

Christensen, U. and Harder, H., Three-dimensional convection with variable viscosity. *Geophys. J. Int.* 1991, **104**, 213–226.

Christensen, U.R. and Yuen, D.A., The interaction of a subducting lithospheric slab with a chemical or phase-boundary. *J. Geophys. Res.* 1984, **89**, 4389–4402.

Christensen, U.R. and Yuen, D.A., Layered convection induced by phase transitions. *J. Geophys. Res.* 1985, **90**, 10291–10300.

Deschamps, F., Li, Y. and Tackley, P.J., Large-scale thermo-chemical structure of the deep mantle: observations and models. In *The Earth's Heterogeneous Mantle*, edited by A. Khan, F. Deschamps, pp. 479–515, 2015. (Berlin: Springer Geophysics).

Fowler, A.C., On the thermal state of the earth's mantle. *J. Geophys.* 1983, **53**, 42–51.

Fowler, A.C., Fast thermoviscous convection. *Stud. Appl. Math.* 1985a, **72**, 189–219.

Fowler, A.C., Secular cooling in convection. *Stud. Appl. Math.* 1985b, **72**, 161–171.

Fowler, A.C., Towards a description of convection with temperature and pressure dependent viscosity. *Stud. Appl. Math.* 1993a, **88**, 113–139.

Fowler, A.C., Boundary layer theory and subduction. *J. Geophys. Res.* 1993b, **98**, 21997–22005.

Fowler, A.C., *Mathematical Geoscience*, 2011. (London: Springer-Verlag).

Fowler, A.C. and O'Brien, S.B.G., Lithospheric failure on Venus. *Proc. R. Soc. London A* 2003, **459**, 2663–2704.

Haskell, N.A., The motion of a viscous fluid under a surface load. *J. Appl. Phys.* 1935, **6**, 265–269.

Jarvis, G.T. and Peltier, W.R., Mantle convection as a boundary layer phenomenon. *Geophys. J. R. Astr. Soc.* 1982, **68**, 389–427.

Jaupart, C., Labrosse, S. and Mareschal, J.C., Temperatures, heat and energy in the mantle of the earth. In *Treatise on Geophysics*, edited by D. Bercovici, Vol. 7, pp. 253–303, 2009. (Amsterdam: Elsevier).

Jimenez, J. and Zufiria, J.A., A boundary layer analysis of Rayleigh–Bénard convection at large Rayleigh number. *J. Fluid Mech.* 1987, **178**, 53–71.

Karato, S. and Wu, P., Rheology of the upper mantle: a synthesis. *Science* 1993, **260**, 771–778.

Khaleque, T., Strongly variable viscosity flows in mantle convection. D. Phil. thesis, University of Oxford, 2015.

Khaleque, T., Fowler, A.C., Howell, P.D. and Vynnycky, M., Numerical studies of thermal convection with temperature- and pressure-dependent viscosity at extreme viscosity contrasts. *Phys. Fluids* 2015, **27**, 076603.

Kirby, S.H., Rheology of the lithosphere. *Rev. Geophys.* 1983, **21**, 1458–1487.

Knittle, E. and Jeanloz, R., Earth's core-mantle boundary: results of experiments at high pressures and temperatures. *Science* 1991, **251**, 1438–1443.
Loper, D.E., A simple model of whole-mantle convection. *J. Geophys. Res.* 1985, **90**, 1809–1836.
Mitrovica, J.X. and Forte, A.M., A new inference of mantle viscosity based upon joint inversion of convection and glacial isostatic adjustment data. *Earth Planet. Sci. Lett.* 2004, **225**, 177–189.
Moore, D.R. and Weiss, N.O., Two-dimensional Rayleigh–Bénard convection. *J. Fluid Mech.* 1973, **58**, 289–312.
Moresi, L.N. and Solomatov, V.S., Numerical investigation of 2D convection with extremely large viscosity variations. *Phys. Fluids* 1995, **7**, 2154–2162.
Moresi, L.N. and Solomatov, V.S., Mantle convection with a brittle lithosphere: thoughts on the global tectonic styles of the Earth and Venus. *Geophys. J. Int.* 1998, **133**, 669–682.
Morris, S. and Canright, D., A boundary layer analysis of Bénard convection in a fluid of strongly temperature-dependent viscosity. *Phys. Earth Planet. Inter.* 1984, **29**, 320–329.
Orth, C.P. and Solomatov, V.S., The isostatic stagnant lid approximation and global variations in the Venusian lithospheric thickness. *Geochem. Geophys. Geosyst.* 2011, **12**, 7. doi:10.1029/2011GC003582.
Paulson, A., Zhong, S. and Wahr, J., Inference of mantle viscosity from GRACE and relative sea level data. *Geophys. J. Int.* 2007, **171**, 497–508.
Reese, C.C. and Solomatov, V.S., Mean field heat transfer scaling for non-Newtonian stagnant lid convection. *J. Non-Newtonian Fluid Mech.* 2002, **107**, 39–49.
Reese, C.C., Solomatov, V.S. and Moresi, L.N., Non-Newtonian stagnant lid convection and magmatic resurfacing on Venus. *Icarus* 1999, **139**, 67–80.
Ricard, Y., Physics of mantle convection. In *Treatise on Geophysics*, edited by D. Bercovici, Vol. 7, pp. 31–87, 2009. (Elsevier: Amsterdam).
Roberts, G.O., Fast viscous Bénard convection. *Geophys. Astrophys. Fluid Dyn.* 1979, **12**, 235–272.
Sammis, C.G., Smith, J.C., Schubert, G. and Yuen, D.A., Viscosity-depth profile of the Earth's mantle: effects of polymorphic phase transitions. *J. Geophys. Res.* 1977, **82**, 3747–3761.
Schaber, G.G., Strom, R.G., Moore, H.J., Soderblom, L.A., Kirk, R.L., Chadwick, D.J., Dawson, D.D., Gaddis, L.R., Boyce, J.M. and Russell, J., Geology and distribution of impact craters on Venus: what are they telling us? *J. Geophys. Res.* 1992, **97**, 13257–13301.
Solomatov, V.S., Stagnant lid convection on Venus. *J. Geophys. Res.* 1996, **101**, 4737–4753.
Solomon, S.C. and Head, J.W., Fundamental issues in the geology and geophysics of Venus. *Science* 1991, **252**, 252–260.
Stein, C. and Hansen, U., Arrhenius rheology versus Frank–Kamenetskii rheology – implications for mantle dynamics. *Geochem. Geophys. Geosyst.* 2013, **14**, 2757–2770.
Tackley, P., Self-consistent generation of tectonic plates in three-dimensional mantle convection. *Earth Planet. Sci. Lett.* 1998, **157**, 9–22.
Tackley, P., Self-consistent generation of tectonic plates in time-dependent, three-dimensional mantle convection simulations. 1. Pseudoplastic yielding. *Geochem. Geophys. Geosys.* 2000a, **1**, 1021. doi:10.1029/2000GC000036.
Tackley, P., Self-consistent generation of tectonic plates in time-dependent, three-dimensional mantle convection simulations. 2. Strain weakening and asthenosphere. *Geochem. Geophys. Geosys.* 2000b, **1**, 1026. doi:10.1029/2000GC000043.
Tackley, P.J., Ammann, M., Brodholt, J.P., Dobson, D.P. and Valencia, D., Mantle dynamics in super-Earths: post-perovskite rheology and self-regulation of viscosity. *Icarus* 2013, **225**, 50–61.
Turcotte, D.L. and Oxburgh, E.R., Finite amplitude convection cells and continental drift. *J. Fluid Mech.* 1967, **28**, 29–42.
Vynnycky, M. and Masuda, Y., Rayleigh-Bénard convection at high Rayleigh number and infinite Prandtl number: asymptotics and numerics. *Phys. Fluids* 2013, **25**, 113602.
Yamazaki, D. and Karato, S., Some mineral physics contraints on the rheology and geothermal structure of Earth's lower mantle. *Am. Miner.* 2001, **86**, 385–391.

Downloaded by [89.234.79.13] at 03:45 10 March 2016

Appendix A

We are concerned with the appropriate boundary condition for the solution of the lid equation (A.1):

$$\frac{s_X}{(1+s_X^2)^2}\exp\left(-\frac{\mu s}{T_a}\right) = \beta D, \tag{A.1}$$

where $D(X)$ (which also depends on s) is determined by (42), χ being the solution of (37). As discussed in the text, this equation is not uniformly valid near $X = a$, and in fact it is not uniformly valid near $X = 0$ either, although it automatically satisfies the zero slope boundary condition. This can be seen by consideration of (26), for example, which shows that the definition of ψ in (29) does not yield zero shear stress at $X = 0$ unless $s_{XXX} = 0$, due to the term $\varepsilon^2\psi_{XX}$. While this is apparently a small term, it is not uniformly so as the viscosity becomes large as we enter the lithosphere.

Some insight can be gained by consideration of a singularly perturbed modification of (A.1),

$$\nu s_{XX} + \frac{s_X}{(1+s_X^2)^2} = \beta D\exp\left(\frac{\mu s}{T_a}\right), \tag{A.2}$$

where we suppose $\nu \ll 1$. First note that the leading order approximation to (A.2) is just (A.1). However, (A.2) has the ability to mimic some features of the corner layer illustrated in figures 5 and 6.

A phase plane analysis of (A.2) is straightforward (in the $(w = s_X, s)$ phase plane), and shows that as X increases, (A.1) is approximately satisfied until $s_X = 1/\sqrt{3} = \tan\pi/6$, following which s begins to rapidly increase, and if D were constant, s would blow up. On the other hand, assuming this is near $X = a$, the discussion earlier indicates that then D must reach zero. Examination of the solution for χ computed assuming s is given by the 0.615 isotherm from the full numerical solution shows that D does indeed approach zero as the slope starts to blow up (figure A1), and the consequence of this is to bring the trajectory back below the s_X-nullcline given by (A.1), and s_X can decrease to a value near zero. This description is illustrated in figure A2.

In more detail, the solution of (A.2) is described in the (w, s) phase plane, where

$$s_X = w, \qquad \nu w_X = \beta D\exp\left(\frac{\mu s}{T_a}\right) - \frac{w}{(1+w^2)^2}; \tag{A.3}$$

trajectories move rapidly to the left hand branch of the w-nullclines, illustrated for values (progressing upwards) of $D = 0.042$, 0.012 and 10^{-7}. As D increases from zero at $X = 0$, the nullclines descend rapidly, and as they do, the solution resides on the left hand stable branch and moves horizontally (since $w \ll 1$) along the inlet adjustment region ab. At the point b, the value of w approaches the maximum value of $1/\sqrt{3} \approx 0.577$. Beyond this value, slow variation of w can only be maintained by having s increase while w remains constant, and this is enabled by having D decrease, as shown in figure A1, which lifts the w–nullcline. This *quasi-static* phase bc is necessary because the cell width (here $a = 3$) is so large.

Eventually, this phase can not be maintained, and a blow-up (cd) occurs, in which

$$\nu s_{XX} \approx \beta D\exp\left(\frac{\mu s}{T_a}\right), \tag{A.4}$$

and this would continue until s becomes infinite, except for the consequent rapid approach of D to zero. When D becomes sufficiently low, the nullcline overtakes the trajectory, so that it reverses direction, and w rapidly decreases towards zero; this is the collapse phase de, in which approximately (for (A.3))

$$\nu s_X^3 s_{XX} + 1 = 0. \tag{A.5}$$

What is the consequence of this for (A.1)? If we supposed that (A.2) was indeed its regularisation, then the requirement of a boundary layer at $X = a$ implies we should require that the outer solution

Downloaded by [89.234.79.13] at 03:45 10 March 2016

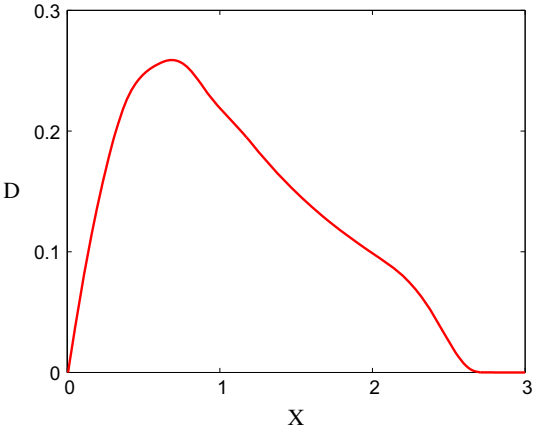

Figure A1. Numerical calculation of $D(X)$ from the solution of (42) for χ with the lid $s(X)$ determined by the full numerical isotherm $T = 0.615$.

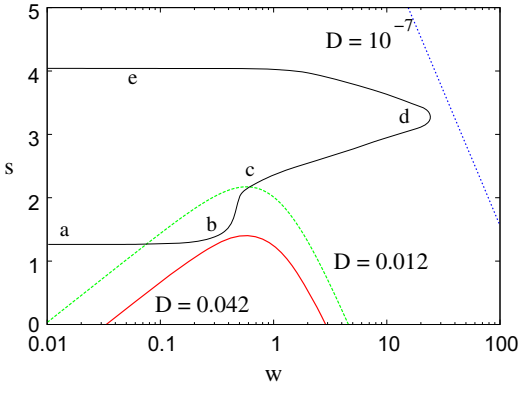

Figure A2. Blow-up and collapse of the slope of the T_a isotherm in the solution of (A.2). The curve *abcde* is the isotherm $T = 0.615$ from the full numerical solution, and consists of four phases: inlet adjustment *ab*, $0 < X < 0.3$, quasi-static *bc*, $0.3 < X < 2.3$, blow-up *cd*, $2.3 < X < 2.8$, and collapse *de*, $2.8 < X < 3$, as described in the text. Also plotted are the (w, s) nullclines given by (A.1) for the indicated values of D.

satisfy

$$s_X = \frac{1}{\sqrt{3}} \qquad \text{at} \qquad X = a. \tag{A.6}$$

We use this idea to close the problem. We formally choose the boundary condition for (A.1) to be (A.6), and this closes the prescription for s. In practice, the numerical solution of (A.1) is done rather differently. We actually solve a regularisation of (A.1) such as that given by (A.2), on the basis firstly that this is a simpler strategy, secondly it may be more accurate than solving (A.1) in comparing with the full numerical solution, and thirdly we solve it as a boundary value problem, using $s_X = 0$ at $X = 0$, and also $s_X = 1/\sqrt{3}$ at the value indicated by the full numerical solution; for $T_a = 0.615$, this is $X = 2.3$. A further problem is that the solution is extremely sensitive to the value of ν. We avoid this difficulty by choosing the value of ν such that in addition, $s(0)$ is the value obtained from the full numerics.

This now raises an additional difficulty. For $T_a = 0.615$, the value of ν we obtain is $\nu = 3.25$, hardly small. Indeed, comparison of figure A2 with figure A1 shows that the "useful" values of D

Downloaded by [89.234.79.13] at 03:45 10 March 2016

are not actually those where the transitions take place, which are $D \approx 0.2$ at b, and $D \approx 0.07$ at c, instead of our indicated values 0.042 and 0.012. The resolution of this awkwardness appears to lie in the choice of regularisation, which is of course not unique. Indeed, if instead we choose a regularisation given by

$$\nu s_{XX} + \frac{s_X}{(1+s_X^2)^2} \exp\left(-\frac{\mu s}{T_a}\right) = \beta D, \tag{A.7}$$

then the choice of ν which provides the correct value of $s(0)$ is $\nu = 0.284$, and we consider this reasonable. This gives the solution shown in figure 7.

On the other hand, while the phase plane up to the quasi-static region is well represented, (A.7) does not permit blow up. A possible compromise to accommodate both effects is the regularisation

$$\nu s_{XX} + s_X \exp\left(-\frac{\mu s}{T_a}\right) = \beta D(1+s_X^2)^2, \tag{A.8}$$

which does permit blow-up. Optimisation of ν to achieve $s(0) = 1.29$ yields $\nu = 0.363$. While it is tempting to pursue even better such terms, it may be a fruitless exercise.

Downloaded by [89.234.79.13] at 03:45 10 March 2016